EXPERIMENTAL STUDY OF A CURVED SLIT SLOW-NEUTRON CHOPPER AND TIME-OF-FLIGHT SPECTROMETER

SILVIO B. HERDADE, LIA Q. DO AMARAL, CLAUDIO RODRIGUEZ and LAERCIO A. VINHAS

PUBLICAÇÃO IEA N.º 136

Fevereiro — 1967

INSTITUTO DE ENERGIA ATÔMICA
Caixa Postal 11049 (Pinheiros)
CIDADE UNIVERSITÁRIA "ARMANDO DE SALLES OLIVEIRA"
SÃO PAULO — BRASIL

EXPERIMENTAL STUDY OF A CURVED SLIT SLOW-NEUTRON CHOPPER AND TIME-OF-FLIGHT SPECTROMETER

Silvio B. Herdade, Lia Q. do Amaral,
Claudio Rodriguez and Laercio A. Vinhas

Nuclear Physics Division
Instituto de Energia Atômica
São Paulo - Brasil

PUBLICAÇÃO IEA Nº 136
fevereiro de 1967

Comissão Nacional de Energia Nuclear

Presidente: Prof. Uriel da Costa Ribeiro

Universidade de São Paulo

Reitor: Prof.Dr. Luiz Antonio da Gama e Silva

Instituto de Energia Atômica

Diretor: Prof. Rômulo Ribeiro Pieroni

Conselho Técnico-Científico do IEA

Prof.Dr.	José Moura Gonçalves	pela USP
Prof.Dr.	José Augusto Martins	pela USP
Prof.Dr.	Rui Ribeiro Franco	pela CNEN
Prof.Dr.	Theodoreto H.I. de Arruda Souto	pela CNEN

Divisões Didático-Científicas

Divisão de Física Nuclear -
Chefe: Prof.Dr. Marcello D.S. Santos

Divisão de Radioquímica -
Chefe: Prof.Dr. Fausto Walter de Lima

Divisão de Radiobiologia -
Chefe: Prof.Dr. Rômulo Ribeiro Pieroni

Divisão de Metalurgia Nuclear -
Chefe: Prof.Dr. Tharcísio D.S. Santos

Divisão de Engenharia Química -
Chefe: Lic. Alcídio Abrão

Divisão de Engenharia Nuclear -
Chefe: Engº Pedro Bento de Camargo

Divisão de Operação e Manutenção de Reatores -
Chefe: Engº Azor Camargo Penteado Filho

Divisão de Física de Reatores -
Chefe: Prof.Dr. Paulo Saraiva de Toledo

Divisão de Ensino e Formação -

EXPERIMENTAL STUDY OF A CURVED SLIT SLOW-NEUTRON CHOPPER AND TIME-OF-FLIGHT SPECTROMETER

Silvio B. Herdade, Lia Q. do Amaral,
Claudio Rodriguez and Laercio A. Vinhas

RESUMO

São apresentadas as características de um espectrômetro de tempo de vôo que utiliza um obturador para neutrons lentos, com fendas recurvadas, em operação num dos canais experimentais do reator IEAR-1 (reator de pesquisas tipo piscina, com potência de 5 MW).

O rotor cilíndrico do obturador contém 9 placas de aço inoxidável recobertas com cádmio, separadas por espaçadores de alumínio, formando 10 fendas recurvadas, e apresenta as seguintes dimensões: abertura lateral total 11 cm x 4,5 cm, raio r = 5 cm, raio de curvatura médio das fendas (valor nominal) R_o = 74,5 cm, largura de cada fenda 0,3968 cm. Um analisador TMC com 1024 canais é usado para a medida dos tempos de vôo que os neutrons lentos levam para percorrer uma distância conhecida do centro do obturador a um detetor de neutrons. Um imã móvel, solidário ao rotor, e uma bobina fixa no suporte do obturador dão origem a um sinal que é utilizado para disparar o analisador multicanal e também para controlar a velocidade de rotação do obturador dentro de 0,5%, através de um sistema que inclui um "ratemeter", um registrador e um relé. As velocidades de rotação utilizadas vão de 2000 a 15000 RPM.

É apresentado um tratamento detalhado das correções para perdas de contagem no sistema detetor e no analisador multicanal.

A calibração do espectrômetro foi realizada ajustando-se de maneira adequada a posição da bobina, no decurso de medidas da secção de choque total de substâncias policristalinas (Fe e grafita), na região onde os degraus de Bragg são observados. Um estudo cuidadoso do efeito da resolução do espectrômetro demonstrou que a posição do ponto de calibração num degrau de Bragg varia de 32,1% a 46,2% da altura total do degrau, quando a resolução varia de 40 a 190 μseg.

A transmissão relativa do obturador $T(\omega\lambda)/T(\omega\lambda)_o$, como uma função do produto da velocidade angular ω(rad/seg) pelo comprimento de onda do neutron λ(Å), foi determinada experimentalmente. Esta função apresenta um máximo para $(\omega\lambda)_o$ = 2700 (rad/seg) Å. A curva que melhor se ajustou aos pontos experimentais foi calculada assumindo-se os valores R_o = 73,32 cm para o raio médio de curvatura das fendas, e r = 4,98 cm para o raio médio do rotor.

A resolução experimental do espectrômetro foi determinada medindo-se o alargamento do degrau de Bragg do Fe(110). É apresentado um cálculo detalhado da função de resolução, para as condições especiais do nosso arranjo experimental. A resolução determinada experimentalmente concorda de maneira satisfatória com a calculada. Obteve-se uma resolução em tempo igual a 2,5% para neutrons de 4,046 Å, com uma velocidade de rotação de 10700 RPM, uma largura de canal de 8 µseg e um detetor de neutrons com uma espessura de 1 polegada.

Foi realizada uma medida da secção de choque total do ouro no intervalo 0,95 Å - 7,00 Å, como um teste adicional de confiança para o espectrômetro, visto êste elemento ser considerado como um padrão para medidas desta natureza.

Programas FORTRAN II-D para o processamento de dados fornecidos pelo espectrômetro de tempo de vôo, e cálculo de secção de choque total, são também apresentados.

RESUMÉ

On présente les caractéristiques d'un spectromètre à temps de vol avec un chopper à plaques courbes pour neutrons lents, utilisé à la sortie d'un des canaux du IEAR-1 (réacteur de récherche type piscine à 5 MW).

Le rotor cylindrique du chopper contient 9 plaques en acier recouvertes de cadmium separées par des entretoises d'aluminium qui forment 10 fentes courbes. Il a les dimensions suivantes: ouverture lateral totale 11 cm x 4,5 cm, rayon r = 5 cm, rayon de courbure moyen nominal des fentes R_o = 74,5 cm, largeur de chaque fente 0,3968 cm. On a utilisé un analiseur TMC à 1024 canaux pour la mesure des temps de vol des neutrons lents parcourant une distance connue du centre du chopper à un détecteur de neutrons. Un aimant mobile, solidaire du rotor et une bobine fixe au soutien du chopper envoyent un signal qui est utilisé pour actionner l'analiseur multicanal et aussi pour controler la vitesse de rotation du chopper à 0,5%, à travers un système qui comprend un "ratemeter", un enregistrateur et un relais.

Les vitesses de rotation utilisées vont de 2000 à 15000 RPM.

On présente un traitement détaillé des corrections pour pertes de comptage dans le système détecteur et dans le multicanal analiseur.

La calibration du spectromètre a été faite en ajustant de façon convenable la position de la bobine lors des mesures de la section efficace totale de substances policristalines (Fe et grafite), dans la région où les seuils de Bragg sont observés. Une étude minutieuse de l'effet de la résolution du spectromètre a demontré que la position du point de calibration dans un seuil de Bragg varie de 32,1% à 46,2% de la hauteur totale du seuil quand la résolution varie de 40 a 190 μ sec.

La transmission rélative du chopper $T(\omega\lambda)/T(\omega\lambda)_o$ comme une fonction du produit de la vitesse angulaire ω (rad/sec) par la longueur d'onde du neutron λ (Å) a été determinée expérimentalement. Cette fonction présente un maximum pour $(\omega\lambda)_o$ = 2700 (rad/sec) Å. La courbe qui s'est mieux ajustée aux points expérimentaux a été calculée en prennant les valeurs R_o = 73,32 cm pour le rayon moyen de courbure des fentes, et r = 4,98 cm pour le rayon moyen du rotor.

La résolution expérimentale du spectromètre a été determinée en mesurant l'élargissement du seuil de Bragg du Fe (110). On présente un calcul détaillé de la fonction résolution dans les conditions spéciales de notre manipulation expérimentale. La résolution determinée expérimentalement est en bon accord avec celle calculée. On a obtenu une résolution en temps égale à 2.5% pour des neutrons de 4.046 Å, avec une vitesse de rotation de 10700 RPM, une largeur de canal de 8 μsec et un détecteur de neutrons avec une épaisseur d'un pouce.

On a fait une mesure de la section efficace totale de l'or dans l'intervalle ..... 0,95 Å - 7,00 Å comme un test en plus de confiance du spectromètre, une fois que cet élement est consideré comme standard dans ce genre de mesures.

On présente aussi des programmes Fortran II-D pour la mise en machine des données obtenues avec le spectromètre à temps de vol et le calcul de la section efficace totale.

ABSTRACT

The experimentally determined characteristics of a curved slit slow-neutron chopper and time-of-flight spectrometer, in operation at a beam hole of the IEAR-1 (5 MW swimming

pool research reactor), are presented.

The cylindrical rotor of the chopper contains 9 cadmium covered steel plates separated by aluminium spacers forming 10 curved slits, and has the following dimensions: total lateral opening 11 cm x 4.5 cm, radius r = 5 cm, nominal average radius of curvature of the slits R_o = 74.5 cm, slit width 0.3968 cm. A TMC 1024 channel analyser is used to measure the time-of-flight of slow neutrons from the center of the chopper to a neutron detector located at a known distance. An electromagnetic pick-up provides a signal that is utilized both to trigger the multichannel analyser and to control the chopper rotational speed within 0.5%, by means of a ratemeter-recorder-relay system. Useful rotational speeds range from 2000 to 15000 RPM.

A detailled treatment of the corrections for counting losses in the detecting system and multichannel analyser is presented.

The calibration of the spectrometer has been carried out by proper adjustment of the magnetic pick-up during the measurements of total cross-sections of polycrystalline substances (Fe and Graphite), in the region where Bragg breaks are observed. A careful study of the effect of the spectrometer resolution has demonstrated that the position of the calibration point in a Bragg break varies from 32.1% to 46.2% of the total height of the break, when the resolution varies from 40 to 190 μsec.

The relative transmission of the chopper $T(\omega\lambda)/T(\omega\lambda)_o$, as a function of the product of the chopper angular speed ω (rad/sec) and neutron wavelength λ (Å), has been determined experimentally. This function has a maximum at $(\omega\lambda)_o$ = 2700 (rad/sec) Å. A calculated curve in which the values R_o = 73.32 cm, for the average radius of curvature of the slits, and r = 4.98 cm, for the average radius of the rotor, were used, provided the best fit to the experimental results.

The experimental resolution of the spectrometer has been determined by measuring the broadening in the Fe (110) Bragg cut-off. A detailed calculation of the resolution function, for the special experimental conditions, is included. A good agreement between the calculated and experimentally determined resolution was observed. The time resolution resulted to be equal to 2.5% for 4.046 Å neutrons, with a chopper speed of 10700 RPM, channel length 8 μsec, and neutron detector thickness of 1 inch.

A total cross-section measurement of gold, in the range of 0.95 Å to 7.00 Å, has been carried out as an additional reliability check of the spectrometer, since this element may be considered as a standard for transmission experiments.

Fortran II-D programs for time-of-flight data processing and for total cross-section computation are also presented.

1. INTRODUCTION

The main objective of this report is to present the experimentally determined characteristics of a curved slit slow-neutron chopper and time-of-flight spectrometer in operation at a beam hole of the IEAR-1 Swimming Pool 5 MW Research Reactor.

The principle of operation of the slow-chopper time-of-flight spectrometer is well known and has been described by many authors(1)(2)(3)(4)(5). A neutron chopper is essentially a rotating collimator that converts a continuous neutron beam into a pulsed one. Each pulse or burst is, in general, formed by neutrons having several different velocities. The time required for these neutrons to reach a detector located at a known distance from the chopper is measured electronically. A magnetic pick-up (or a photoelectric device) connected to the rotating chopper provides a signal each time a neutron burst is formed at the center of the rotor. This signal determines the zero of the time scale by triggering an electronic clock or multichannel time analyser, that accumulates counts in different channels corresponding to different neutron velocities.

The original Fermi slow-chopper consisted of several straight slits formed by neutron absorbing parallel plates. A curved slit neutron chopper can provide a crude monochromatization of the beam, in addition to its pulsing action.

The apparatus described in the present report has been devised primarily for the utilization in slow-neutron scattering experiments applied to solid and liquid state physics. Nevertheless, it can be also used in the determination of neutron spectra and nuclear cross-sections of interest to the reactor physicist.

The present report includes a total cross section measurement of gold as an additional reliability check of the spectrometer, since this element may be considered as a standard for this kind of experiment.

2. DESCRIPTION OF THE SPECTROMETER

A block diagram of the time-of-flight spectrometer is shown in figure 1. It consists of 5 main systems:

a) curved slit slow-neutron chopper;
b) analyser trigger and speed control system;
c) spectrometer neutron detecting system;
d) multichannel time-of-flight analyser;
e) neutron beam monitor.

Curved slit slow-chopper

The curved slit slow-neutron chopper has been built at the Instituto de Energia Atômica workshop following a design developed at the Swedish AB Atomenergi, kindly forwarded to us by Dr. K. E. Larsson[4][6]. The basic theory of the instrument has been worked out in detail by Larsson et al[4]. The apparatus (figure 2) consists essentially of a cylindrical rotor - A,B,C - housed in a steel box - D. An Universal electronic motor (ELECTRON Type MU/100, 110 V, 1.2 Amp, 100 W, 15000 RPM), the axis of which is connected directly to the axis of the rotor by means of an elastic coupling, can rotate

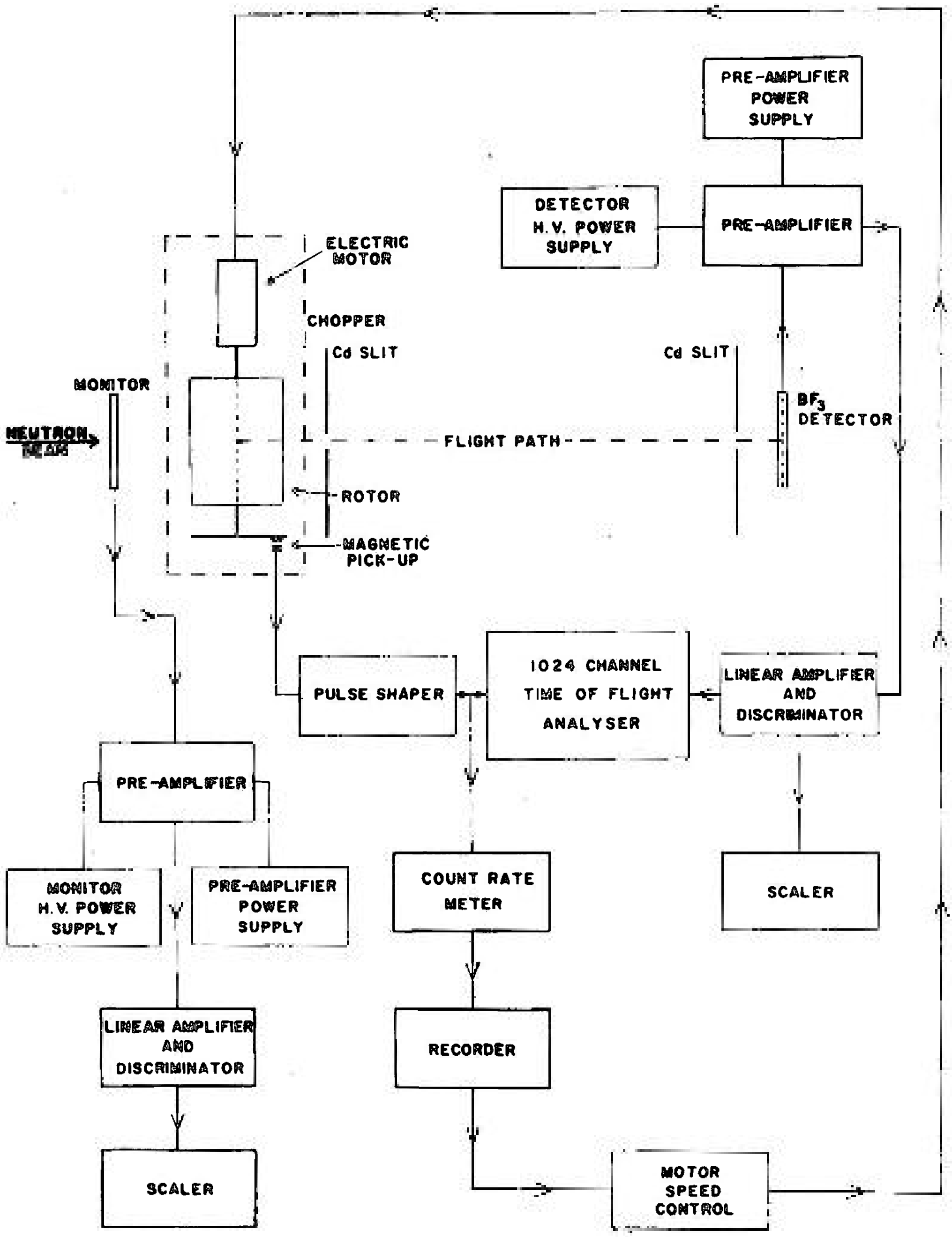

Figure 1 - Block diagram of the time-of-flight slow neutron spectrometer.

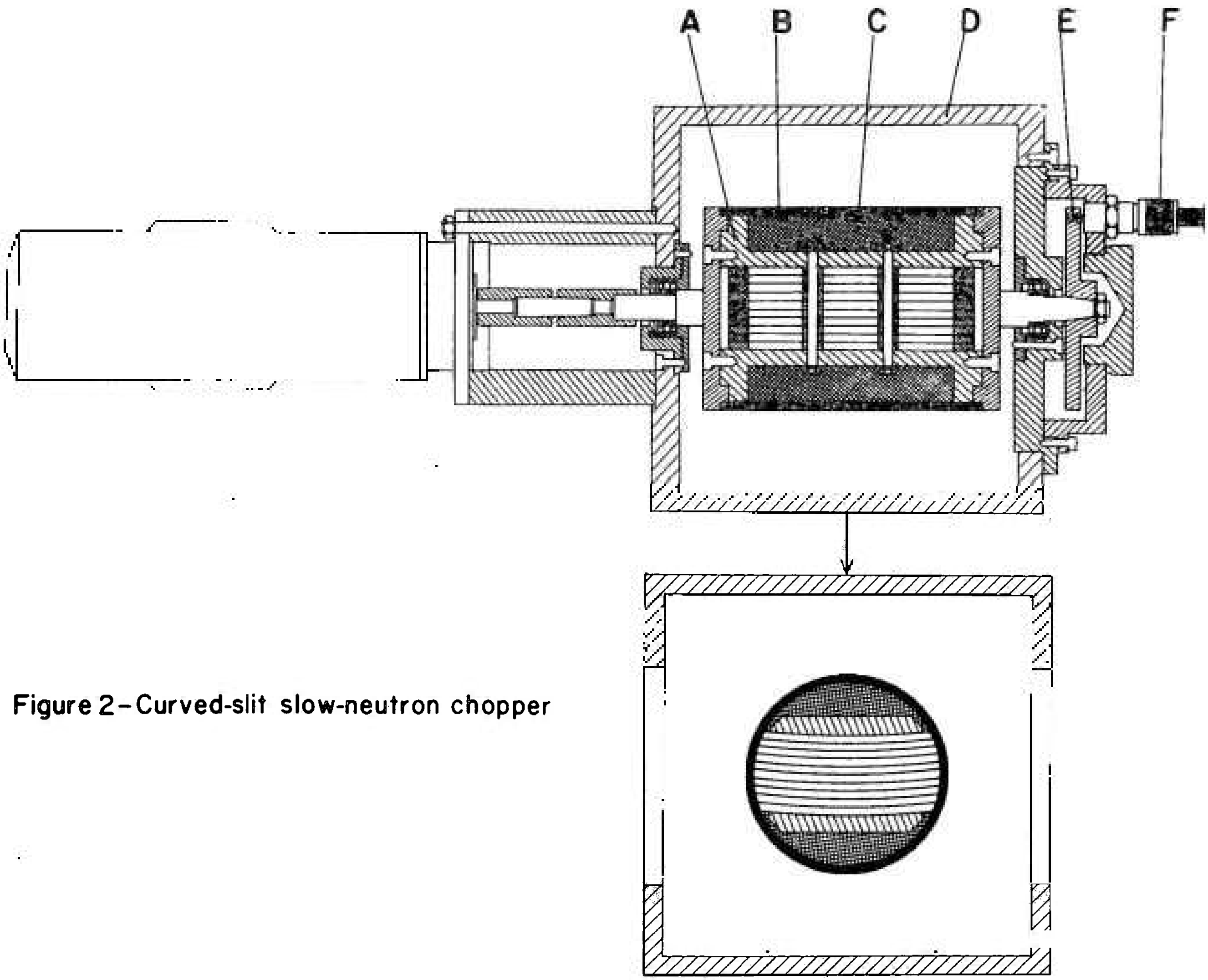

Figure 2–Curved-slit slow-neutron chopper

the chopper with speeds up to 12000 RPM. With the use of a grinder Universal motor (LESTO 8201, 110 V,280 W, 27000 RPM) the chopper can be operated with speeds until 15000 RPM. The rotor contains nine cadmium covered steel plates separated by aluminium spacers forming 10 curved slits. These plates are 0.5 mm thick and the thickness of cadmium deposited in both surfaces is ~ 55 micra. The remaining volume - C - of the cylinder, outside the slits, is filled with B_4C mixed with "Araldite" in approximately equal amounts. An aluminium sleeve - B - fits over the slit assembly and neutron absorbing material closing the lateral surface of the rotor.

The dimensions used are the following:

- chopper total lateral opening: 11 cm x 4.5 cm
- chopper radius: r = 5 cm
- average radius of curvature of the slits: R_o = 74.5cm
- slit width (distance between Cd covered steel plates): 2d = 0.3968 cm.

Analyser trigger and rotor speed control system

An electromagnetic pick-up coil - F - (figure 2),actuated by a small permanent magnet in the aluminium disk E, provides a signal that is utilized both to trigger the time-of-flight multichannel analyser and to control the chopper rotational speed. The position of the magnet relative to the rotor can be adjusted so that it passes right in front of the fixed pick-up in the moment a neutron burst is formed in the center of the chopper. A fine adjustment can be attained by means of a micrometer screw that changes slightly the position of the pick-up coil. The motion of the small magnet passing across the pick-up coil builds up a signal that may be used to trigger the time analyser (zero of time scale). The amplitude and form of this signal change with the chopper speed as is shown in figure 3(a). Such wave forms do not

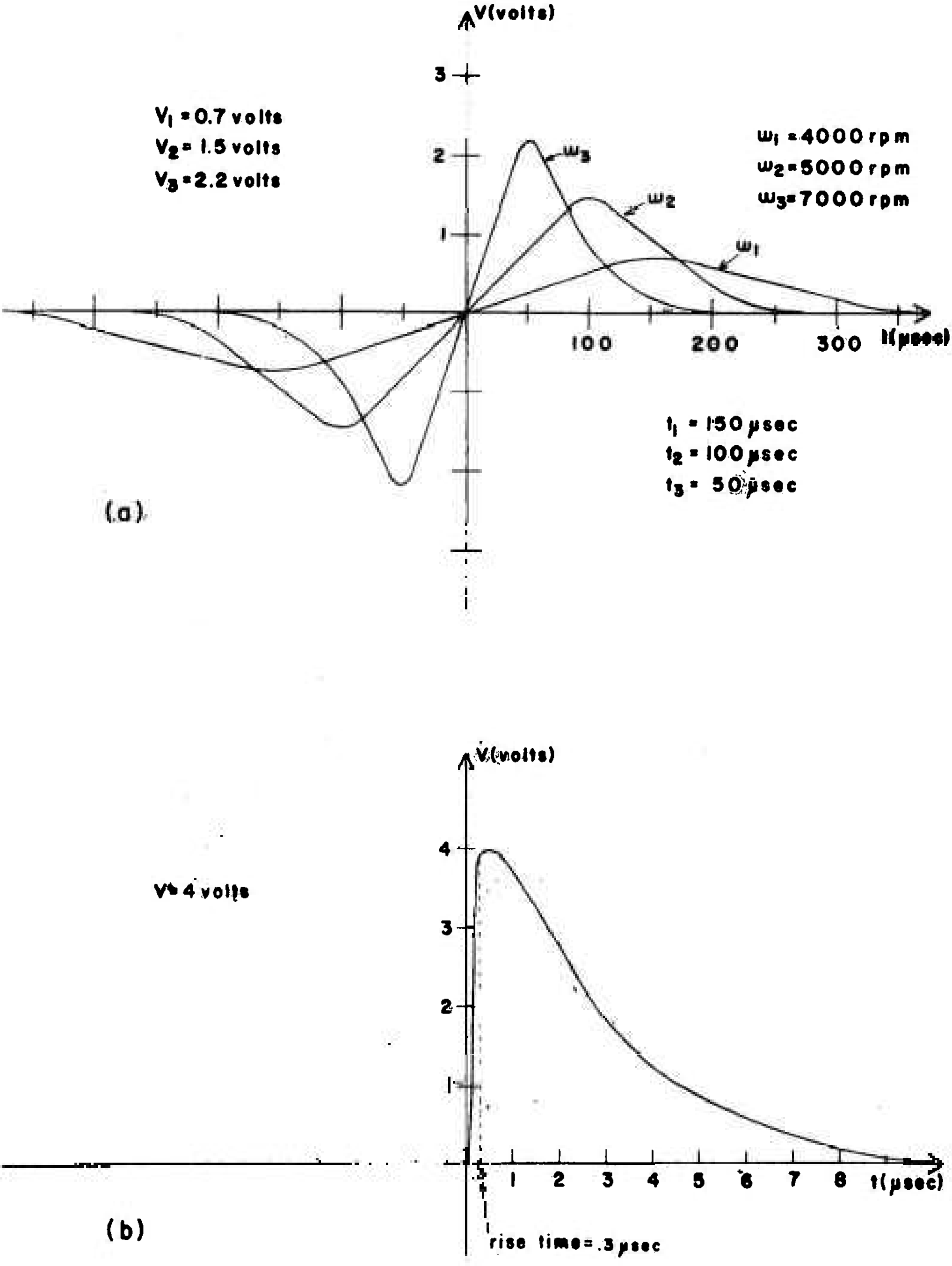

Figure 3 - a) Magnetic pick-up wave form. The trigger voltage is approximately 0.015 volts.

b) Out-put pulse from pulse shaper.

satisfy the requirements of the analyser trigger input: a positive pulse of amplitude 3 to 10 volts and rise time 0.5 micro seconds. So, a pulse shaping circuit (figure 4) has been devised by one of us to convert the electromagnetic pick-up wave form into a more convenient pulse shape. This circuit is a modified transistor monovibrator presenting an output positive pulse of 4.1 volts, with 0.3 microseconds rise time (figure 3-b), and it is triggered by the magnetic pick-up signal whenever its polarity changes in crossing the zero axis. Carefull measurement of the exact trigger point gave a trigger voltage of about 0.015 volts. The change in the chopper speed introduces only a negligible variation in the trigger time.

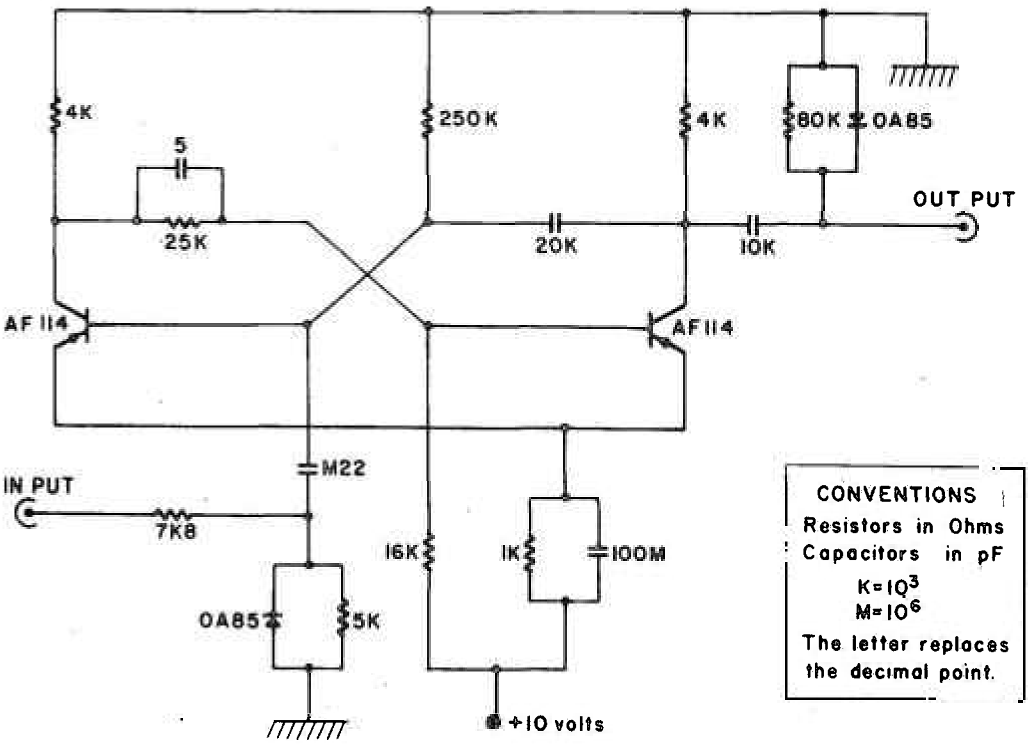

Figure 4 - Trigger signal pulse shaper.

The output pulse of the pulse shaping circuit goes to the trigger input of the multichannel time analyser and also to a scaler and ratemeter (BRASELE, Mod. CDCR 1a) that actuates a chart recorder (MECI-Leeds & Northrup). This system indicates the rotational speed of the chopper in RPM. The rotational speed is controlled by a relay (figure 5) that switches on and off the chopper electric motor and is actuated by the indicator of the chart recorder. In this way the speed can be controlled within 0.5% during several hours of operation.

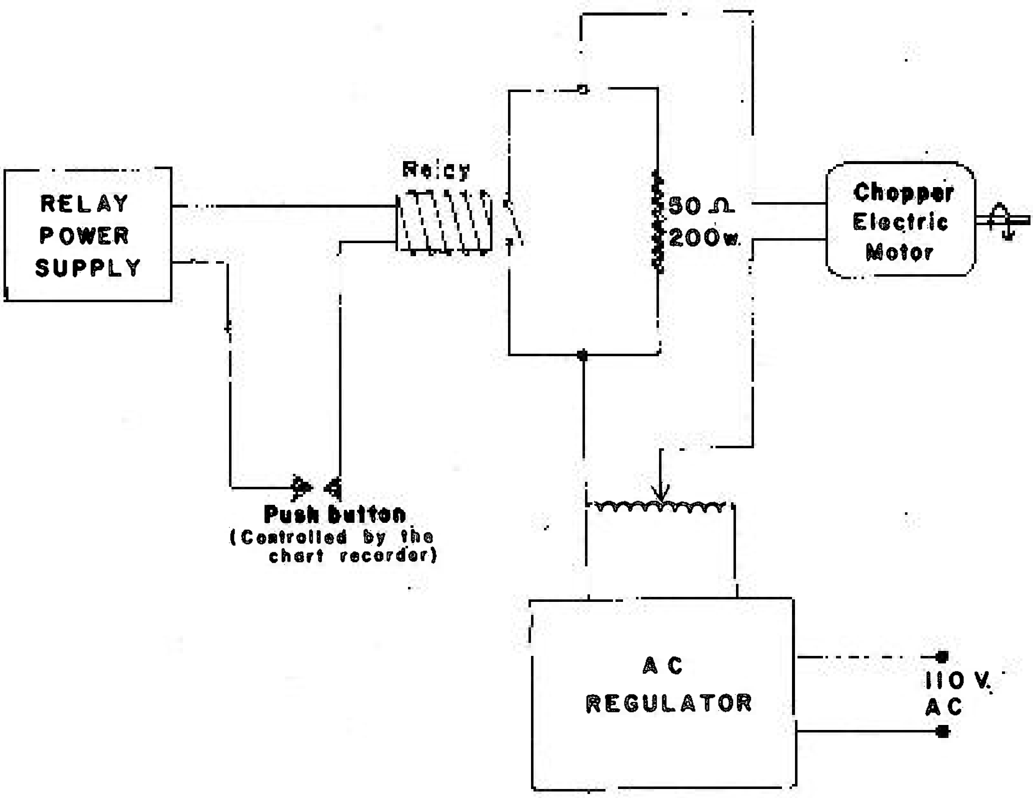

Figure 5 - Relay circuit for rotor speed control.

Spectrometer neutron detecting system

Neutrons coming in bursts from the chopper are detected by one (or more) counters located at a known distance. The following neutron detecting system has been utilized, in the measurements of the chopper and spectrometer characteristics:

- N.Wood Model G-10-12 $B^{10}F_3$ detector 1" diameter x 12" length, 60 cm Hg gas pressure, 96% enriched in B^{10} ;
- IEA - SE preamplifier (figure 6);
- Amplifier and discriminator BRASELE Mod. AA 1c 1d (this unit has been modified to give a negative output pulse of 500 mV, to satisfy the requirements of the multichannel analyser signal input).

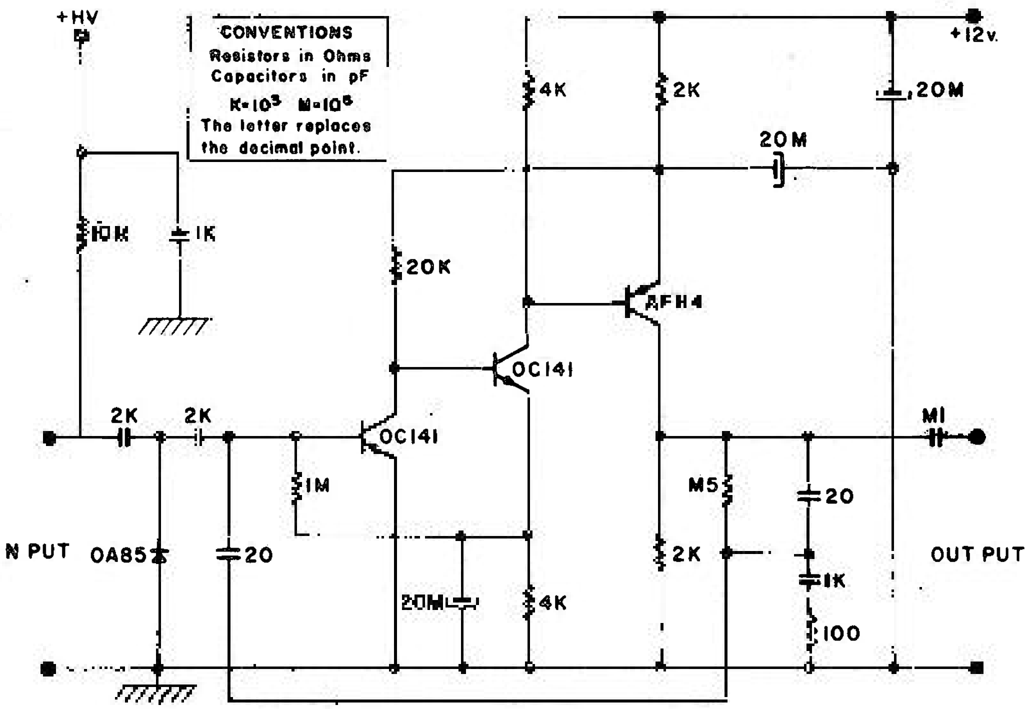

Figure 6 - BF_3 preamplifier.

- Low voltage power supply BRASELE Mod FEBT 2a (modified to give 10 volts for the transistorized preamplifier).
- H.V. power supply MESCO Type A PN 5003, 6 KV full scale, for the BF_3 counter.

Multichannel time-of-flight analyser

The apparatus used is a TMC 1024 channel analyser. With the Model 211 Time-of-Flight Logic Unit plugged in, the Model CN-1024 system is capable of making neutron energy measurements by determining the arrival time of a detector pulse with respect to the time of release of a neutron burst (as determined by the magnetic pick-up system). With a known source-to-detector distance and the neutron flight time measured as above, neutron velocities and hence energies or wavelengths are readily determined. Channel lengths of 0.25, 0.5, 1, 2, 4, 8, 16, 32, and 64 microseconds can be selected.

The full memory of the analyser (1024 channels),half the memory (512 channels), or 1/4 of the memory (256 channels) may be utilized. Active time (number of channels used multiplied by the channel length) can be set for the range of interest and to prevent flight time measurement of particles with lower energies. A delay, equal to 0, 1, 2 or 3 times the active time, can be set to prevent flight time measurement of particles with higher energies than those of interest. The Instruction Manual for the Model 211 Unit also indicates a fixed delay: one channel, with 0.25 to 16 microsecond channel lengths; 16 microseconds, with 32 or 64 microsecond channel lengths, plus additional 0.1 microsecond delay for each successive channel.

The nominal dead time of the analyser is 16 microseconds. Corrections for counting losses in the spectrometer will be treated in APPENDIX I.

FORTRAN programs for data processing have been prepared and are presented in APPENDIX II.

An experimental check of the performance of the CN-1024 Multichannel Analyser, with the Time-of-Flight Logic Unit plugged in, has been carried out with the equipment shown in figure 7.

For all channel lengths the measured dead time was 16 microseconds.

For 0.25 to 16 microseconds channel length the first channel has been found to have zero length (does not accept pulses);

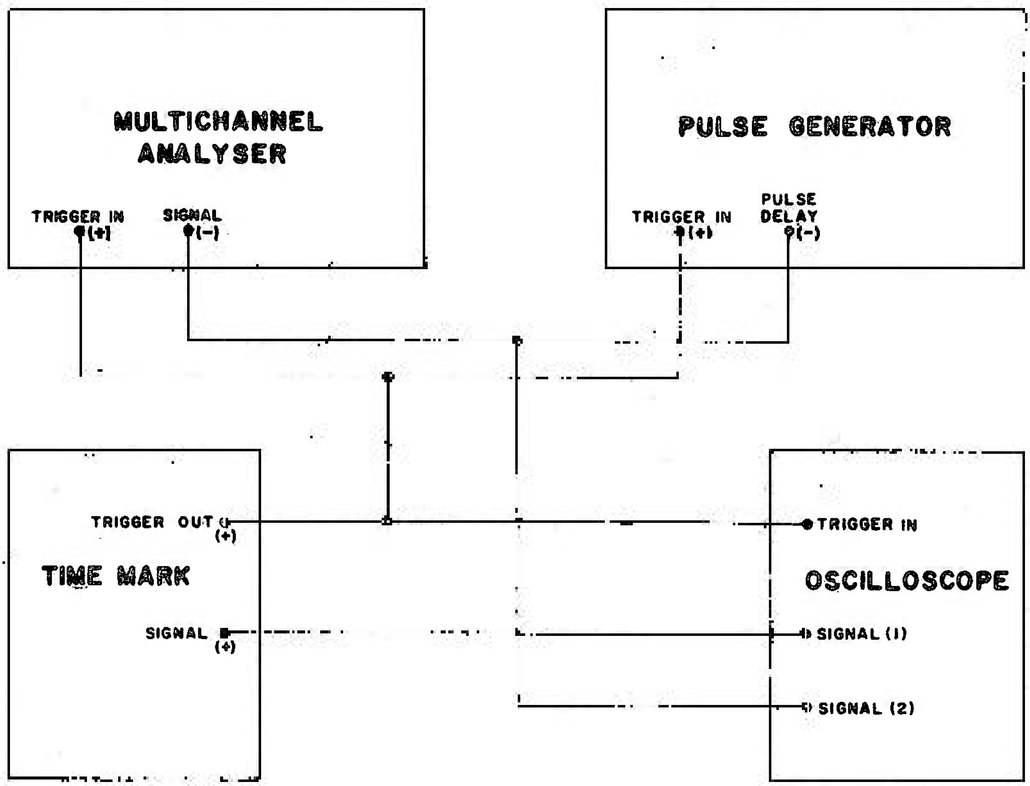

Figure 7 - Block diagram of the equipment utilized in the check of the performance of the CN-1024 multichannel analyser.

the second channel accepts pulses from 1 to 1 + ΔT microseconds (ΔT = channel length), the third channel from 1 + ΔT to 1 + 2 ΔT microseconds, and so on. For these channel lengths the analyser can count up to 1 pulse per channel per cycle of analysis.

For 32 microseconds channel length, the first channel accepts pulses from 1 to 17 microseconds; the second channel accepts pulses from 17 to 17 + ΔT, the third from 17 + ΔT to 17 + 2 ΔT, and so on. The analyser can count 1 pulse per channel per cycle.

For 64 microseconds channel length, the first channel accepts pulses from 1 to 49 microseconds; the second from 49 to 49 + ΔT, the third from 49 + ΔT to 49 + 2 ΔT, and so on. The analyser can count 2 pulses per channel per cycle.

The above results of the experimental check of the Multichannel Analyser do not quite agree with the information contained in the Instruction Manual concerning the fixed delay. The additional 0.1 microsecond delay for each successive channel could not be observed experimentally.

The experimental behaviour of the time analyser has been taken into account in the calibration of the time scale.

For slow neutron spectrometry the most used channel lengths are 8, 16 and 32 microseconds. All the resolution studies presented in section 7 have been carried out with ΔT = = 8 microseconds.

<u>Neutron beam monitor</u>

A small low efficiency BF_3 detector was placed before the chopper to monitor the continuous reactor neutron beam, as is shown schematically in figure 1. The monitor detecting system consists of:

- N. Wood Microneutron BF_3 detector, 1/4" diameter x

1" length, 30 cm Hg gas pressure, depleted (11% B^{10});

- IEA - SE Preamplifier (figure 6);
- Amplifier and Discriminator BRASELE Mod AAI 1c 1d;
- Scaler BRASELE Mod CDI 2a.

3. EXPERIMENTAL ARRANGEMENT

The experimental arrangement that has been utilized for the measurement of the chopper and spectrometer characteristics is shown in figure 8.

The IEAR-1 Swimming Pool Reactor[7][8], operating at 2 MW has been used as a neutron source. The chopper was placed in front of a through tube (tangential beam-hole Nº 13) so that the reactor core is not seen directly, the neutron source being a volume of moderator (H_2O) contained in the portion of the through tube located in front of the core. A collimator made of a mixture of boric acid and a plastic material, designed for another experiment, has been maintained inside the beam hole. The neutron beam at the source has a circular cross-section with a diameter of 15 cm and it narrows down to a rectangular opening with dimensions of 2.5 x 1.0 cm, at the reactor wall end of the through tube.

At the chopper position the thermal neutron flux is $2 \times 10^8 n/cm^2.sec$, and the cadmium ratio is 16, as measured with gold foils.

The distance from the center of the neutron source to the center of the chopper is 330 cm. A 12" long x 1" diameter BF_3 detector is placed at a known distance in front of the chopper. The chopper axis of rotation and the detector are both in the horizontal position and parallel to each other. Flight paths of 1.50 m and 3.00 m have been used.

Three cadmium slits s_1, s_2, s_3 are located in the

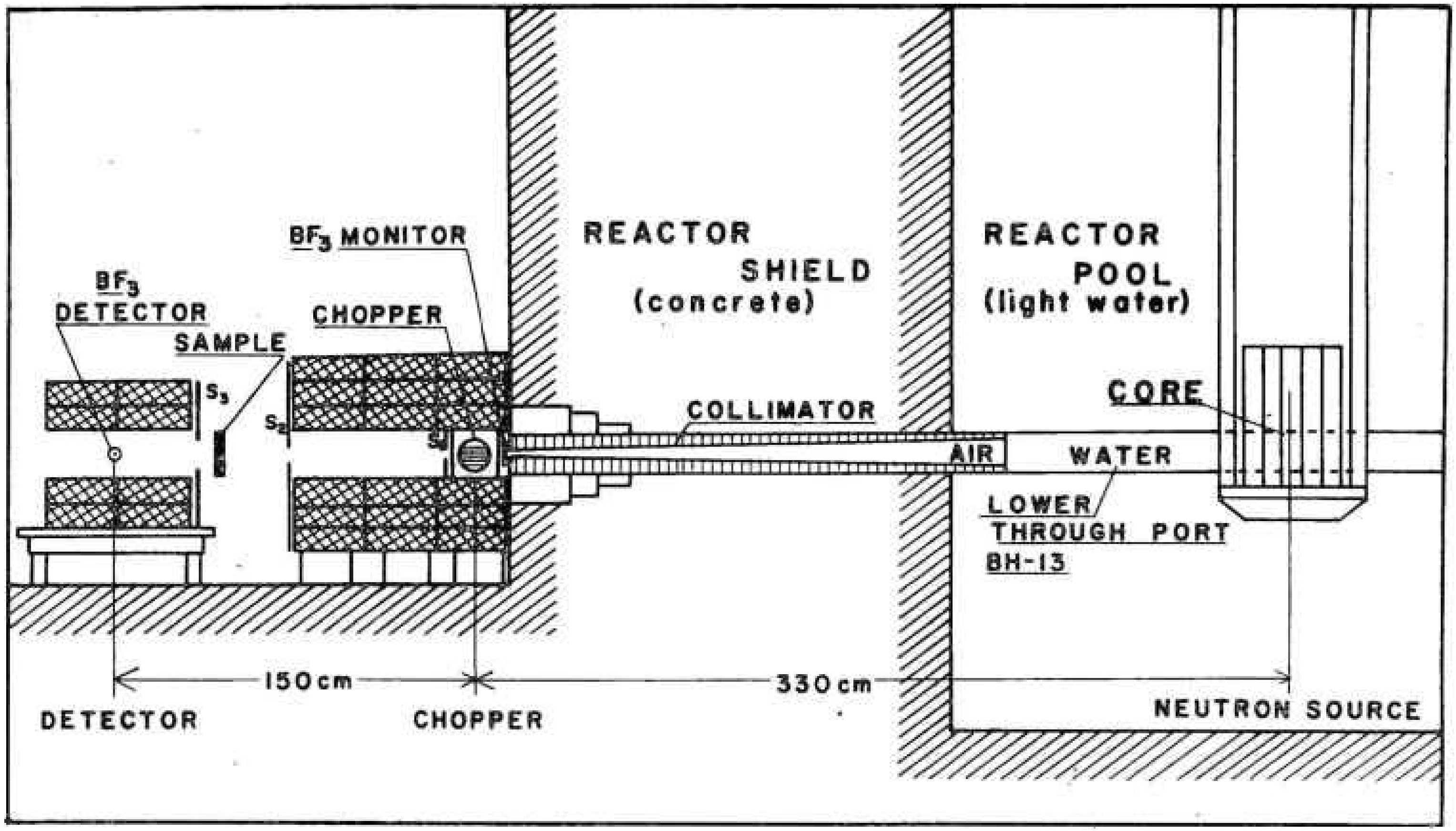

Figure 8 - Experimental arrangement utilized for the measurement of the chopper and spectrometer characteristics.

positions indicated by figure 7.

A small low efficiency BF_3 detector (99% transmission for 2200 m/sec neutrons) 1" long x 1/4" diameter is located between the opening of the beam and the chopper for monitoring the neutron intensity.

Wood boxes 5 x 10 x 40 cm filled with paraffin and boric acid are used as neutron shields for the chopper and detector. A beam-catcher, not shown in figure 8, stops the reactor beam after its passage through the detector.

The utilization of just one 1" detector and the above mentioned collimator do not provide the best efficiency for a given resolution of the spectrometer.Nevertheless, this arrangement resulted to be satisfactory for preliminary experiments using the direct reactor beam in which the intensity is not a serious problem. A specially designed collimator and a detector bank will be used in the definitive spectrometer installation,in connection with a cooled Beryllium filter,for inelastic scattering experiments.

4. CALIBRATION OF THE TIME-OF-FLIGHT SCALE

The calibration of the time scale of the spectrometer is carried out by sending through the chopper neutrons of a well known wavelength. The time analyser is triggered by a pulse from an electromagnetic pick-up. When the calibration is correct the measured time-of-flight should agree exactly with the calculated one, independently of the chopper speed, what means that the position of this pick-up must be adjusted in such a way that the analyser is triggered exactly when the neutron burst is formed in the center of the chopper.

If the magnet does not pass across the coil exactly in the same instant on which the neutron burst is formed in the center of the chopper, the pick-up pulse will be formed a fraction of a revolution later (or earlier) corresponding to an angular shift $\Delta\phi$. This angle $\Delta\phi$ is constant for a given position of the pick-up, but the zero point in the time scale will vary with the angular velocity of the chopper, and that is the main factor which contributes to the variation of the zero of the time scale with the chopper speed. In this case, the zero of the neutrons will differ from the zero of the pick-up by a Δt_1 proportional to $1/\omega$, according to the relation $\Delta t_1 = \Delta\phi / \omega$.

The position of the pick-up must be adjusted in order to make this angle $\Delta\phi$ equal to zero.

Another fact that must be taken into account is that the pulse shaping circuit is triggered when the magnetic pick--up signal reaches the trigger voltage; the trigger time changes with ω (see figure 3(a)). This gives a contribution Δt_2 to the variation of the zero of the time scale with the chopper speed. Nevertheless, a careful experimental analysis of the triggering point for various chopper speeds has shown that this error varies between 0 and 2 μsec, being therefore negligible.

The zero time calibration was made independent of the chopper speed by the following procedure: the total cross section of polycrystalline iron has been measured in the region of the Fe(110) Bragg cut-off, with a flight path of 1.49m and for various chopper speeds. The position of the pick-up was adjusted until reprodutibility of the measured time-of-flight for calibration was stablished for all chopper speeds within 4 μsec.

A careful total cross-section measurement was made to minimize the influence of the nearest aluminium break and to define precisely the position of the 4.046 Å cut-off corresponding to neutrons with a time-of-flight of 1023.2 μsec/m. The influence of the spectrometer resolution and of the shape of the total cross section curve on the determinationof the exact point corresponding to the cut-off wavelength is discussed in detail in APPENDIX III.

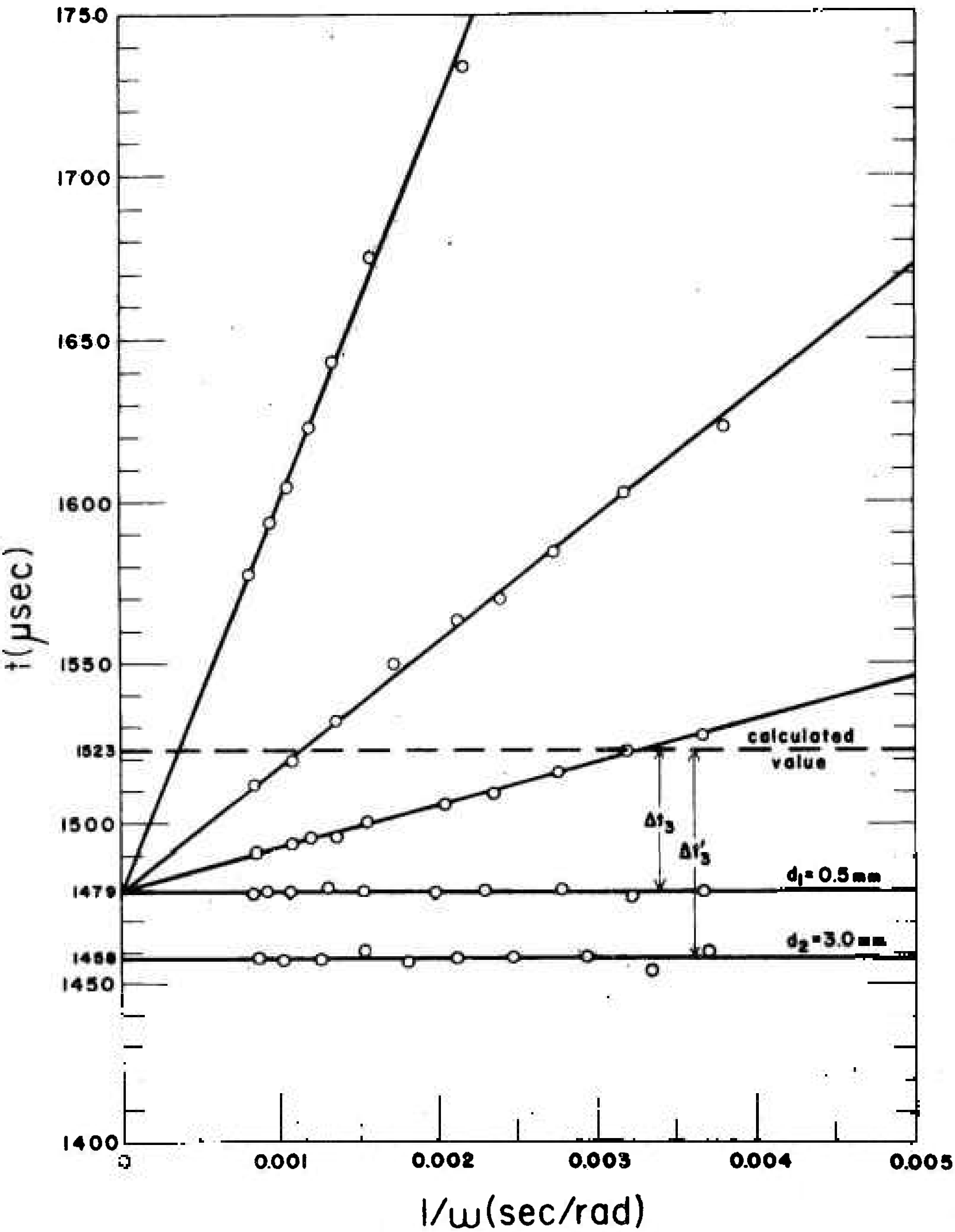

Figure 9 - Calibration curves as a function of $1/\omega$ obtained with the Fe(110) Bragg cut-off (flight path of 1.49 cm). The final position of the pick-up coil gives Δt_3 = 44 μsec.

The experimentally obtained time-of-flight of the neutrons corresponding to the Bragg cut-off was plotted against $1/\omega$. The straight line thus obtained should pass through the calculated value for $1/\omega = 0$. In order to obtain a good calibration it is necessary to cover a wide range of ω values for the definition of the slope of this straight line with good accuracy. By successive adjustments of the pick-up we can arrive to a calibration that is, to a good approximation, independent of the chopper speed. This can be seen in figure 9, where successive calibration curves using the Fe(110) cut-off are shown as a function of $1/\omega$.

It was also observed that the measured time-of-flight did not agree exactly with the calculated one, even if this calibration point did not change with the chopper speed. A fixed displacement Δt_3 was observed, and seems to be independent of ω, but varies with the distance between the pick-up coil and the disk where the moving small magnet is located. By varying this distance along the perpendicular to the disk, it was observed a change of the calibration point. This Δt_3 increases with the pick-up coil to disk distance as is shown in figure 9, where results are presented for two distances, 0.5 mm and 3.0 mm.

After the final adjustment of the pick-up, measurements at different neutron wavelengths have been carried out using other Fe breaks and the graphite (0002) Bragg cut-off. It was observed that the calibration is independent of neutron wavelength. The position of the breaks was constant with the chopper speed and the same Δt_3 shift was observed. This experimentally determined Δt_3 has been introduced as an additive correction for the time scale.

A FORTRAN II-D program for conversion of channel number to time-of-flight, wavelength and energy is presented in APPENDIX II.

5. BACKGROUND

The chopper described in the present report has been designed for thermal and subthermal neutron experiments;resonance and fast neutrons will pass right through the cadmium slits as if the rotor contained just one large opening. In order to demonstrate this fact, a cadmium plate with a thickness sufficient to stop all thermal neutrons has been placed between chopper and detector, so that a pulsed beam of epi-thermal neutrons reaches the detector. This pulsed beam of epi-thermal neutrons gives a time dependent contribution to the spectrometer background.Another time dependent contribution comes from thermal neutrons scattered by the rotor, the sample and the shield. This contribution can be minimized by covering with cadmium the detector area not reached by the direct beam, and by using several cadmium slits along the flight path. Finally, there is another contribution - the room background - which is time independent and can be minimized by the use of a convenient shield around the detector.

The spectrum of neutrons that have passed through a 0.7mm thick cadmium absorber, with the chopper rotating at 5240 RPM was measured with a channel length of 8 μsec and a flight path of 1.49m and is shown in figure 10. This curve presents two maxima that correspond to the 0º and 180º open positions of the rotor. Between these maxima we can see big flat regions corresponding to the time independent room background. The narrow peaks I and II are due to the fine collimation provided by our experimental arrangement,which produces a beam with a cross section 1.00 x 2.50cm at the chopper location, and therefore smaller than the chopper total opening 11.00 x 4.50cm. Hence, only a few central chopper slits are utilized at the rotor positions corresponding to the maximum transmission. On both sides of these peaks we can notice small valleys a, b, c, that are caused by the variation of the angle of incidence of the beam on the chopper curved slits with the angular position of the rotor, which determines a variation of the cadmium thickness traversed. The differences in shape of the 0º and 180º bursts, and the assymetry observed are due to the fact that the chopper slits are curved.

From the time difference between the value of the abcissa corresponding to the maximum of the 180º burst and the one corresponding to the half period of rotation of the chopper, the average energy of the epi-thermal neutrons in the beam has been estimated as being 1.16 ev.

The width of both the 0º and 180º epi-thermal neutron bursts varies with the chopper speed.

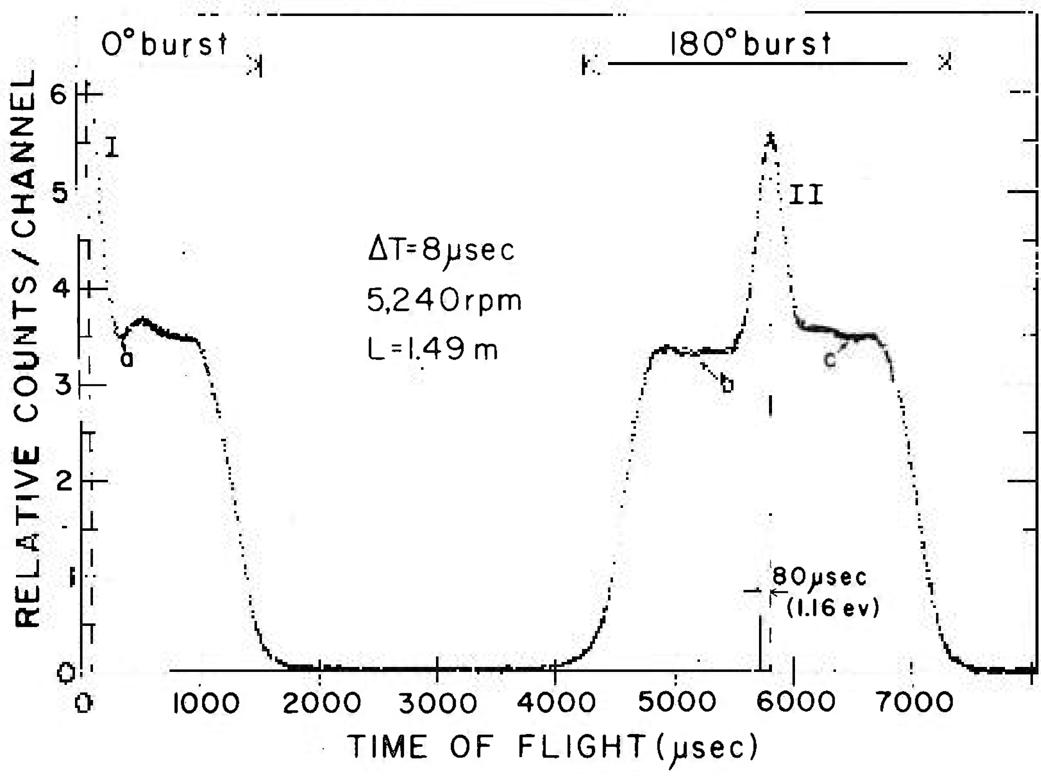

Figure 10 - Neutron background.

In direct beam experiments, such as total cross section measurements, care should be taken in using spectra that fall in the low background region between the 0° and 180° bursts. This can be achieved by choosing convenient chopper rotating speeds and by varying the length of the flight path.

The direct beam epi-thermal background can be reduced by using filters inside the reactor collimator.

6. THE CHOPPER TRANSMISSION FUNCTION

The chopper transmission, or the probability per unit time for the passage of a neutron through it, is a function, $T(t,v)$, of the neutron velocity and the instant t the neutrons pass through the center of the chopper.

The study of the chopper transmission as a function of time can be reduced to the study as a function of the angle of incidence α between the neutron path and the chopper slits in a rotating reference system connected to the chopper and with the t axis coinciding with the axis of rotation(4). This study has been carried out with detail for the case of a cylindrical chopper with effective radius r, curved slits with a radius of curvature R_o, slit width 2d, and angular speed ω (4)(9). The function $T(t,v)$ or $T(\alpha,v)$ presents the following properties:

a) it is symmetrical about the angle

$$\alpha^* = r \left| \frac{2\omega}{v} - \frac{1}{R_o} \right| \quad ;$$

b) it is a triangle with a basis $2d/r$ for $v = v_o$ and when its contribution for the resolution of the apparatus is studied it can be approximated for all velocities by a triangular function with the same basis. The value v_o is given by the condition

$$\alpha^* = 0, \quad \text{or} \quad v_o = 2\,\omega\, R_o ,$$

The chopper transmission as a function of the neutron wavelength λ and of the angular speed ω can be obtained by integrating the function $T(t,v)$ with respect to time or the function $T(\alpha,v)$ with respect to the angle α, and replacing v by $h/m\lambda$, where h is Planck's constant and m is the mass of the neutron. The results are as follows:

$$T(\omega\lambda) = \begin{cases} \frac{d}{r} \left[1 - \frac{2}{3} \frac{r^4}{d^2} \frac{m^2}{h^2} (\omega\,\Delta\,\lambda)^2 \right] \\ \qquad \text{for} \quad 0 \leq \omega\,\Delta\,\lambda \leq \frac{d}{2r^2} \frac{h}{m} \\ \frac{8}{3} \sqrt{2 \frac{m}{h} d \;\omega\,\Delta\,\lambda} - 4 \frac{m}{r} r\,\omega\,\Delta\,\lambda + \frac{2}{3} \frac{m^2}{h^2} \frac{r^3}{d} (\omega\,\Delta\,\lambda)^2 ; \\ \qquad \text{for} \quad \frac{h}{m} \frac{d}{2r^2} \leq \omega\,\Delta\,\lambda \leq \frac{h}{m} \frac{2d}{r^2} \end{cases}$$

with: $\Delta\lambda = |\lambda - \lambda_o|$. $\lambda_o = \frac{h}{m} \frac{1}{2\,\omega\, R_o}$.

A new burst of neutrons is emitted after the chopper has been rotated 180º. In this case the transmission is still given by the above expressions, but now $\Delta\lambda = |\lambda + \lambda_o|$.

From the formulae above, the minimum velocity and correspondingly the maximum wavelength of the neutrons that are transmitted by the chopper in the 0º position can be determined:

$$v_{min} = 2\,\omega \left(\frac{r^2 R_o}{4\,d\,R_o + r^2} \right) ,$$

$$\lambda_{max} = \frac{h}{m} \frac{1}{2\omega} \left(\frac{4 d R_o + r^2}{r^2 R_o} \right) .$$

The maximum flight path, that is the flight path for which the slowest neutron can reach the detector just before the chopper opens again, the overlap of cycles of analysis being avoided, is given by

$$\ell_{max} = \frac{2\pi}{\omega} v_{min} = 4\pi \left(\frac{r^2 R_o}{4 d R_o + r^2} \right) .$$

As the chopper transmission is a function of the product $\omega\lambda$, if one of the variables is fixed, the transmission as a function of the other variable is obtained.

The transmission curve can be obtained experimentally by several methods, the simplest one consisting in the study of how a known neutron spectrum is deformed after being transmitted by the chopper at a constant rotating speed. Unfortunately, the wavelength distribution of thermal neutrons in the lower tangential channel (BH-13) of the IEA-R1 reactor was not known with precision. So, an alternative method consisting in the study of the transmitted intensity as a function of ω , for a certain neutron wavelength, has been chosen for the experimental determination of the chopper transmission function. In this method, wavelengths λ and rotation speeds ω must be chosen so that the range of interest is covered. With this in mind, the chopper speed has been varied from 2500 RPM to 11000 RPM and neutron wavelengths from 0.806 Å to 8.185 Å have been taken. For each wavelength of the reactor spectrum the transmitted intensity as a function of $\omega\lambda$ gives a curve proportional to the transmission curve. If many different wavelengths are considered a family of curves is obtained. These several curves after normalization give the experimental transmission function.

The experimental curves have been obtained in such a way

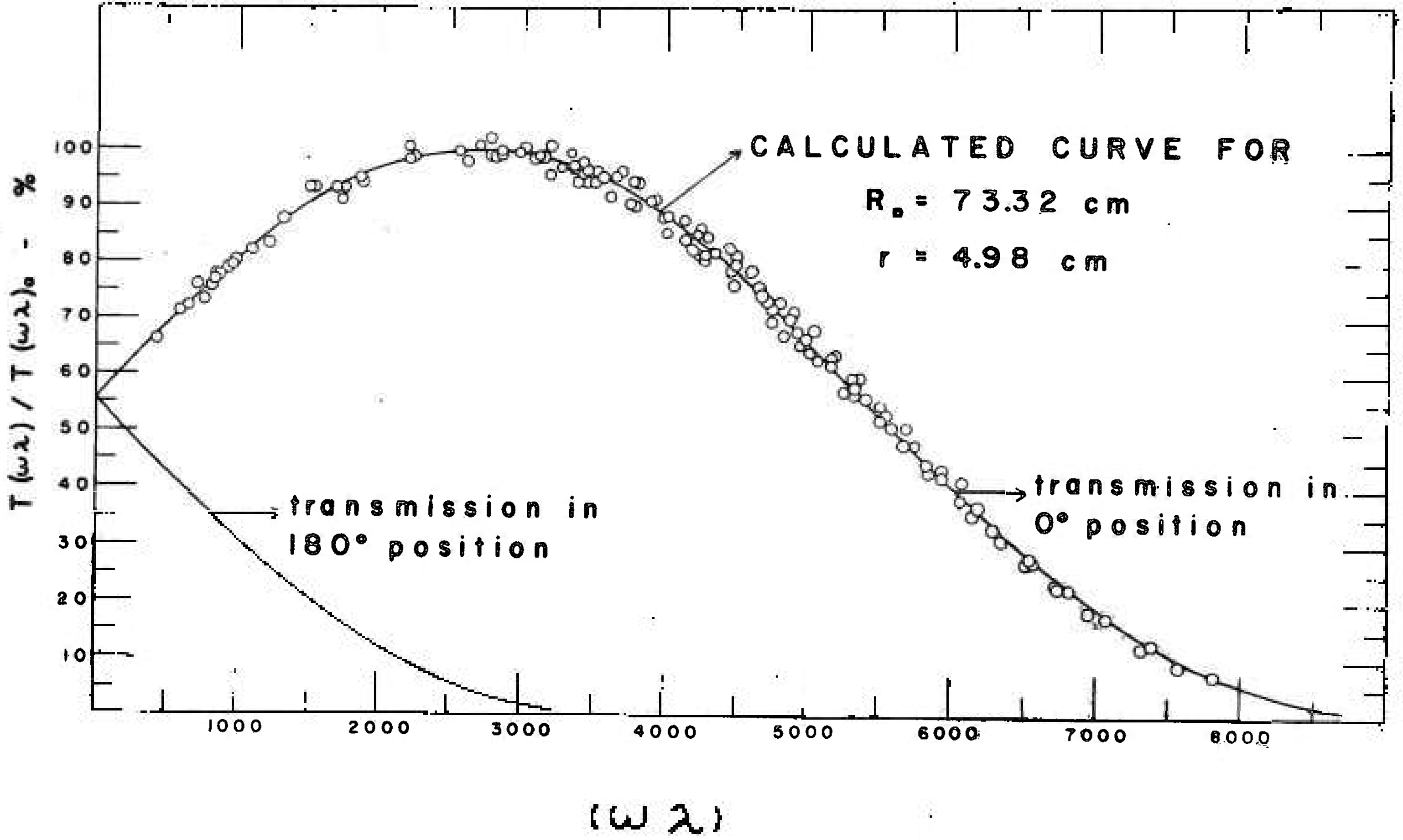

Figure 11 - The relative chopper transmission as a function of ($\omega\lambda$).

as to present regions of overlap in order to make easier the experimental normalization.

In order to minimize resolution effects which are dependent on λ and ω , the wavelengths that have been chosen came from smooth regions of the reactor spectrum.

For the experimental determination of the chopper transmission function the $\omega\lambda$ interval from 400 to 7.800 Å.rad/sec has been covered with 29 curves which included 134 experimental points.

A theoretical curve has been calculated, which gave the best fit to the normalized experimental points, using numerical values for r, 2d and R_o. As already mentioned in a previous section of this report, the IEA slow-chopper has the following dimensions: r = 5.00cm, 2d= 0.3968cm, R_o= 74.5cm. The effective radius of the chopper, i.e., the mean radius of the slits traversed by the neutron beam utilized is equal to 4.98cm, as the collimation is such that the beam covers just a few central slits.

The radius of curvature R_o has been determined from the maximum of the experimental transmission curve corresponding to the abcissa $(\omega\lambda)_o$= 2700 Å.rad/sec resulting a R_o= 73.32cm. This result presents an apparent deviation of 1.6% from the nominal design value R_o = 74.5cm.

The calculated transmission curve that gave the best fit to the experimental points was the one in which the values r = = 4.98cm, 2d = 0.3968cm and R_o= 73.32cm have been used. The various experimental curves were normalized again to this calculated curve, and the final result is presented in figure 11. The agreement between the experimental points and the theoretical curve is quite satisfactory. Using these values for r, 2d and R_o, the minimum transmitted neutron velocity, v_{min}, the maximum transmitted wavelength, λ_{max}, and the maximum flight path without overlap, ℓ_{max} have been

$$v_{min} = 0.438\,\omega \text{ m/sec}$$
$$\lambda_{max} = 9040/\omega \text{ Å}$$
$$\ell_{max} = 2.752 \text{ cm}$$

7. RESOLUTION

Two different contributions must be considered in the study of the overall resolution of the chopper and time-of-flight spectrometer: one that depends on the chopper angular speed, its parameters and on the geometry of the system, and another one that is due to the detector finite thickness and the channel width of the time analyser.

The essential geometry of the spectrometer is shown in figure 12. A neutron emitting surface with a diameter $2D_1$ is located at a distance L_1, and a neutron detecting surface with a diameter $2D_2$ is located at a distance L_2 from the center of the chopper. As the chopper rotates its slits sweep over the neutron emitting area. The beam collimation or the angular width of the chopper burst is determined by the angular opening of the chopper $2d/r$ and by the smaller of the two angles

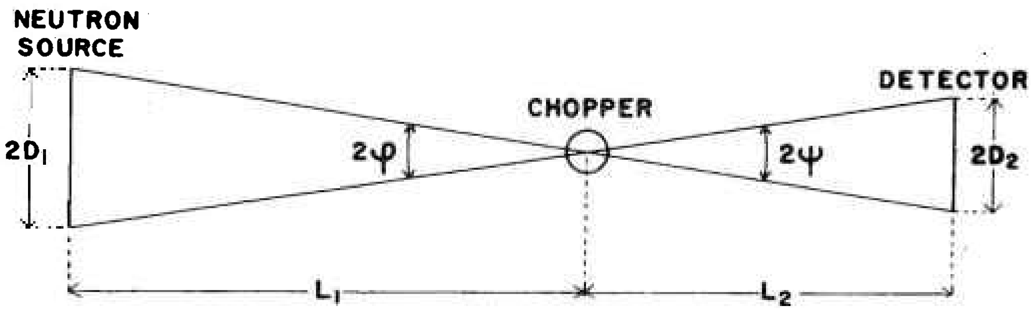

Figure 12 - Essential geometry of the spectrometer.

$$2\psi \simeq \frac{2D_1}{L_1} \qquad \text{and} \qquad 2\psi \simeq \frac{2D_2}{L_2} \quad .$$

This smaller angle will be denoted simply by 2D/L.

The neutron flux at the source is in general a function of the position in the emitting surface and of the neutron velocity. However, in what follows a constant neutron flux over the entire effective emitting surface and a constant efficiency for the detecting surface will be assumed. Under these conditions, the neutron intensity transmitted through the chopper is given as a function of the angle of incidence by[4]

$$I(\alpha',v) = \int_{\alpha' - \frac{d}{r}}^{\alpha' + \frac{d}{r}} T(\alpha - \alpha',v)\, I_o(\alpha ,v)\, d\alpha \ ,$$

where α' is an angle that varies with the chopper sweeping action over the emitting area and

$$I_o(\alpha ,v) = \begin{cases} A(v) \ , & \text{for } |\alpha| \leq D/L \\ 0 \ , & \text{for } |\alpha| \geq D/L \end{cases}$$

Let us restrict to the case $v = v_o$, in which the transmission function $T(\alpha - \alpha', v_o)$ is a triangle with a basis $2d/r$ and symmetrical about α'. The transmitted intensity $I(\alpha',v_o)$ will be given by the composition of the rectangular function $I_o(\alpha)$ swept by the function $T(\alpha - \alpha')$, as is shown in figure 13. The resultant normalized function $I(\alpha',v_o)$ depends on the relative widths of the triangle and of the rectangle as follows:

<u>Case a</u> : $2D/L \geq 2d/r$

In this case the maximum transmission is equal to 1 and the full width at half maximum is given by 2D/L and, hence, it is independent of the chopper opening angle.

Case b : $d/r \leq 2D/L \leq 2d/r$

In this case the maximum transmission is $\leq$ 1 and the full width at half maximum is given by[4]:

$$2\,\bar{\alpha} = \left(\frac{2D}{L} + \frac{2d}{r}\right) - 2\sqrt{\left(\frac{d}{r}\right) - \left(\frac{d}{r} - \frac{D}{L}\right)^2}$$

and hence it varies in the interval $2d/r \geq 2\,\bar{\alpha} \geq (3 - \sqrt{3})d/r$.

Case c : $2D/L \leq d/r$

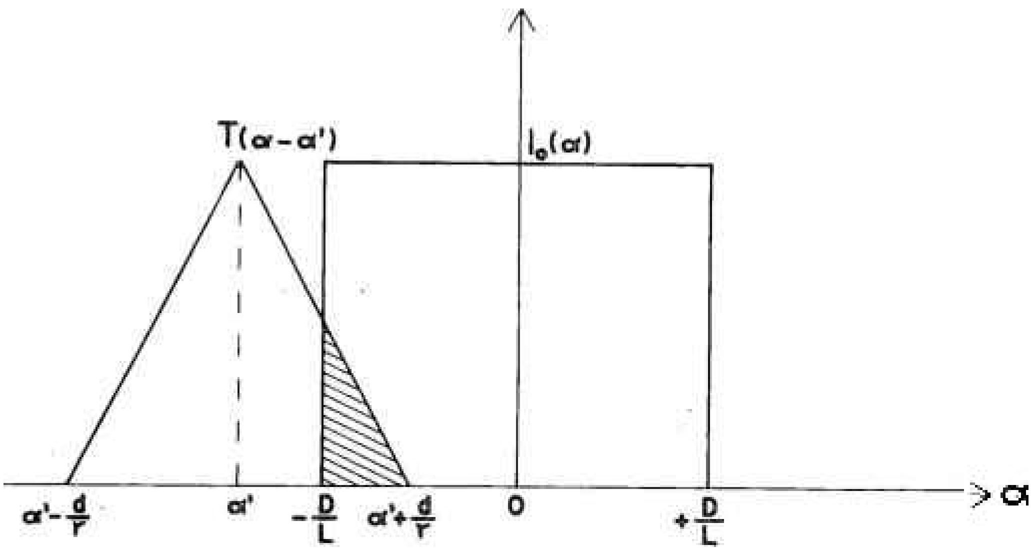

Figure 13 - Rectangular function $I_o(\alpha)$ swept by the function $T(\alpha - \alpha')$.

This last case has not been treated in detail in reference (4), as the corresponding gain in resolution is relatively small when compared with the loss in intensity. However, this was the case for the preliminary experimental arrangement used as mentioned in part 3 of this report. Since for transmission experiments the intensity is not a serious problem, just one 1" thick detector has been used so that $2D/L < d/r$.

A detailed calculation of the function $I(\alpha', v_o)$ can be found in APPENDIX IV. In this case the maximum transmission is less than 1 and the full width at half maximum is:

$$1)\quad 2\bar{\alpha} = 2\left(\frac{d}{r} + \frac{D}{L}\right) - 2\sqrt{\frac{D}{L}\left(\frac{2d}{r} - \frac{D}{L}\right)}$$

$$\text{for}\quad \frac{4}{5}\frac{d}{r} \leq \frac{2D}{L} \leq \frac{d}{r}$$

$$\text{and varies in the interval}\quad 1.2\,\frac{d}{r} \leq 2\bar{\alpha} \leq (3-\sqrt{3})\,\frac{d}{r}$$

$$2)\quad 2\bar{\alpha} = \frac{d}{r} + \frac{D}{2L} \qquad \text{for}\quad \frac{2D}{L} \leq \frac{4}{5}\,\frac{d}{r}$$

$$\text{and, hence,}\quad 2\bar{\alpha} \leq 1.2\,\frac{d}{r}\ .$$

In the experimental arrangement utilized, the beam collimation was determined by the detector, and for a flight path $\ell = 1.5m$, $2D/L = 0.0156$. As $d/r = 0.0401$, case 2 above applies .

The resolution function $I(\alpha', v_o)$ has been calculated using the formulae derived in APPENDIX IV and is shown in figure 14. The result is a curve having a maximum in 0.3512 and full width at half maximum $2\bar{\alpha} = 1.097\ d/r = 0.044$. Nevertheless, this curve cannot be approximated by a Gaussian with the same width at half maximum and consequently another approximation has been used. As it can be seen by the integration of the resolution function, the area under the curve is equal to the area of the triangle shown by dashed line in figure 14, with maximum $(2D/L)(r/d) = 0.389$ and basis $2d/r = 0.0802$ and has a value $2D/L$.

The full width at half maximum of a Gaussian with the same area having a maximum at 0.3512 has been calculated giving the result $\Gamma_{1/2} = 1.04\ d/r$. The curve $I(\alpha')$ has been approximated by the Gaussian obtained in the above described way.

All the calculations have been carried out for $v = v_o$.

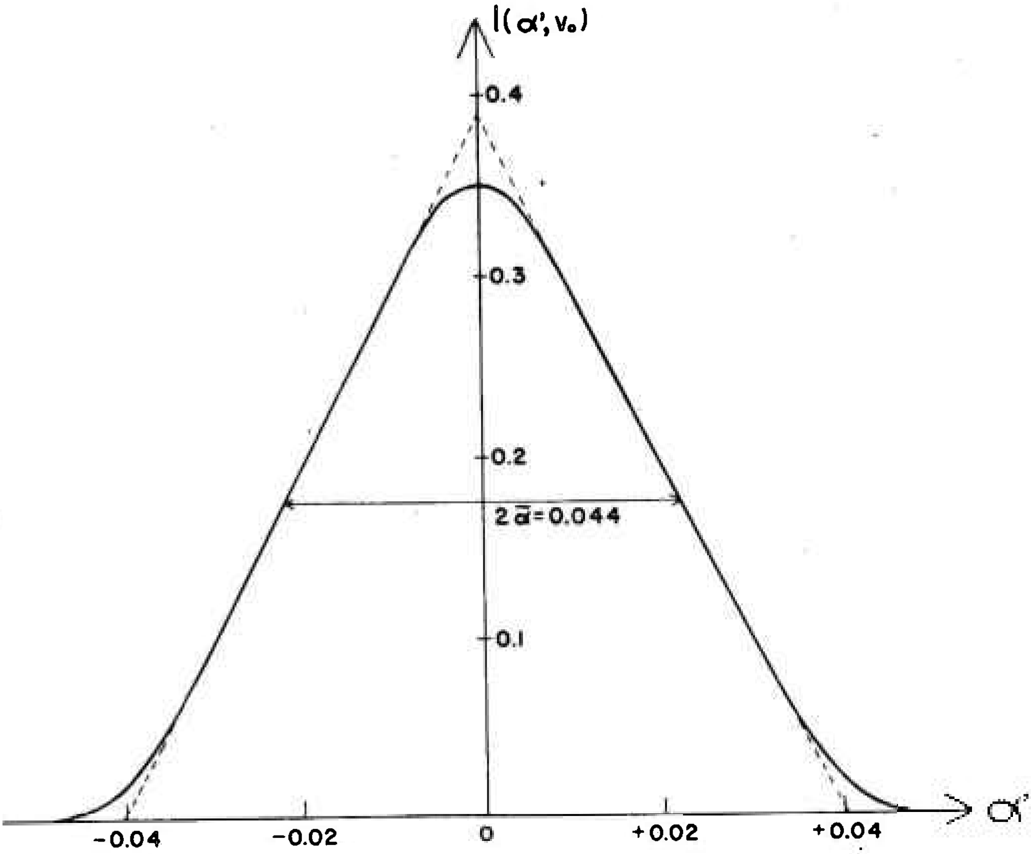

Figure 14 - Resolution function $I(\alpha', v_o)$.

For $v \neq v_o$ small deviations may be observed as the transmission function in this case is not exactly triangular.

If the result is expressed in a time scale we have

$$\delta t_\omega = 1.04 \frac{d}{\omega r} ,$$

where ω is the chopper rotating speed.

The other contributions to the resolution are due to the average time spent by the incoming neutron to cross the counter thickness and to the time analyser channel width. If the detector have an effective thickness d_1, neutrons with a velocity v will spend a time $\delta t_d = d_1/v$ to cross this thickness. Let δt_c be the analyser channel width. If these two contributions are approximated by Gaussian functions, the following expression can be written for the spectrometer overall resolution:

$$\delta t = \sqrt{\delta t_\omega^2 + \delta t_d^2 + \delta t_c^2}$$

or

$$\delta t = \sqrt{(1.04 \frac{d}{\omega r})^2 + (\frac{d_1}{v})^2 + \delta t_c^2} .$$

The total neutron cross-section of polycrystalline iron has been measured, as a function of neutron wavelength, in the region of the 110 Bragg cut-off, for the experimental determination of the spectrometer overall resolution.

Theoretically, the Bragg cut-off in a total cross-section curve should have a zero slope. However, the finite width of the spectrometer resolution rounds off the edges of the curve and the cut-off slope assumes a non zero value. Figure 15 shows the results for two different chopper speeds: 5355 RPM and 10050 RPM.

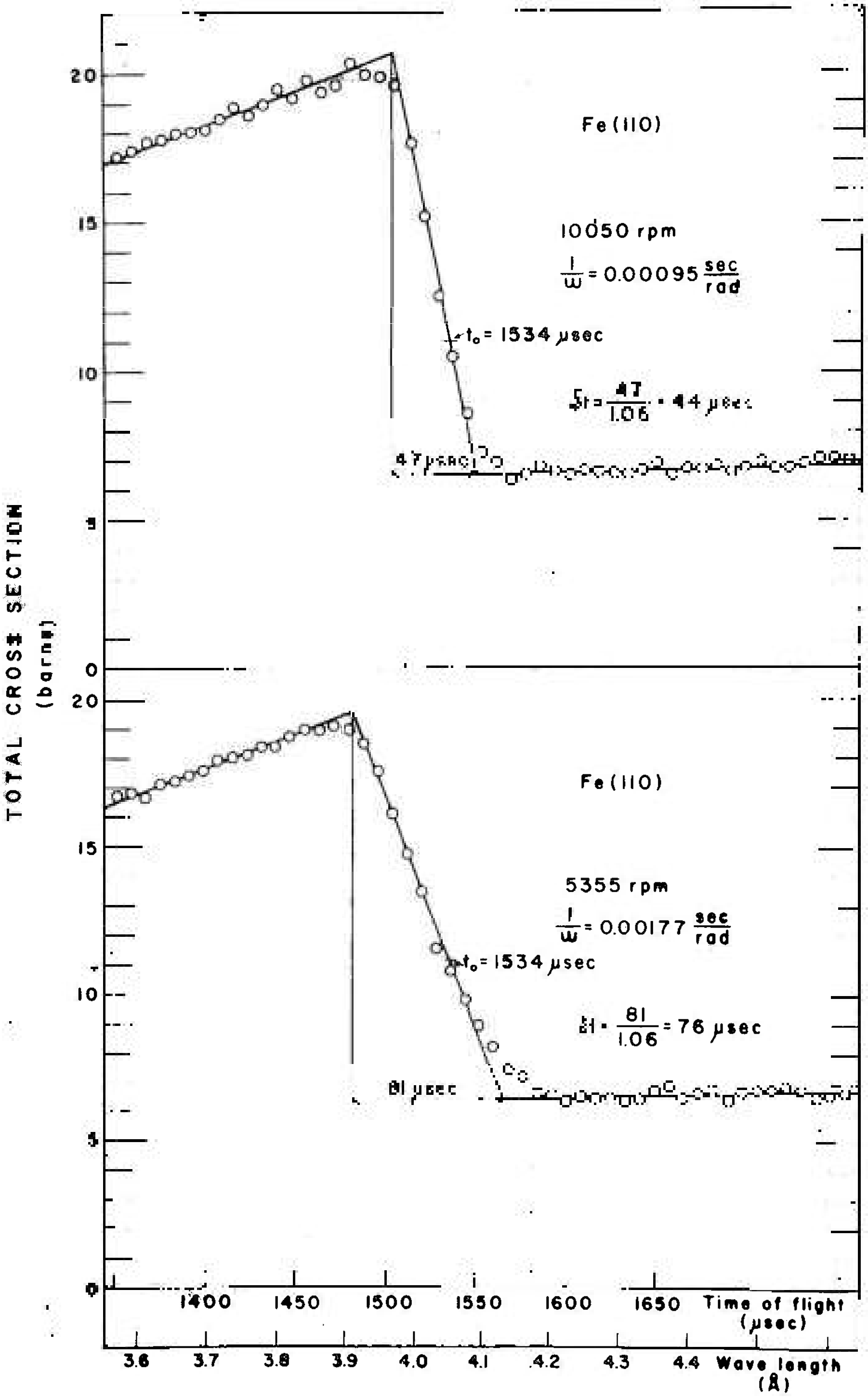

Figure 15 - Fe(110) Bragg cut-off for different chopper speeds: 10050 RPM and 5355 RPM.

The projection of the tangent at the point of inflexion of the experimental cut-off determined as shown in figure 15 has the value of 1.06 times the full width at half maximum δt, as it has been derived in APPENDIX III for our conditions.

The 110 Bragg cut-off of polycrystalline iron at 4.046 Å has been studied experimentally with several chopper rotating speeds. The experimental results for δt as a function of $1/\omega$ are given in Table I.

TABLE I

EXPERIMENTAL WIDTH δt AS A FUNCTION OF $1/\omega$ FOR 4.046 Å NEUTRONS (with $\delta t_c = 8\ \mu sec$)

SAMPLE (*)	CHOPPER SPEED RPM	$1/\omega$ rad^{-1} sec	δt μsec	$\delta t/t$
Fe - 1	10,701	0.00089	38 ± 4	2.5 %
Fe - 2	10,050	0.00095	44 ± 4	2.8 %
Fe - 1	7,887	0.00121	53 ± 4	3.4 %
Fe - 2	7,035	0.00135	58 ± 4	3.8 %
Fe - 1	6,400	0.00149	60 ± 5	3.9 %
Fe - 2	5,355	0.00177	76 ± 5	4.9 %
Fe - 1	4,800	0.00200	85 ± 5	5.5 %
Fe - 1	4,193	0.00228	94 ± 6	6.1 %
Fe - 1	3,635	0.00263	113 ± 7	7.4 %
Fe - 1	2,830	0.00338	147 ± 7	9.6 %
Fe - 1	2,362	0.00404	167 ± 8	10.9 %

The detector used was a $B^{10}F_3$ counter, 60 cm Hg gas pressure, with an internal diameter of 2.34cm. This detector can be considered "thin" in the sense that its self-screening effect is negligible, and so ist effective thickness is the mean

(*) Fe - 1 = Armco type forged iron; Fe - 2 = Powdered iron

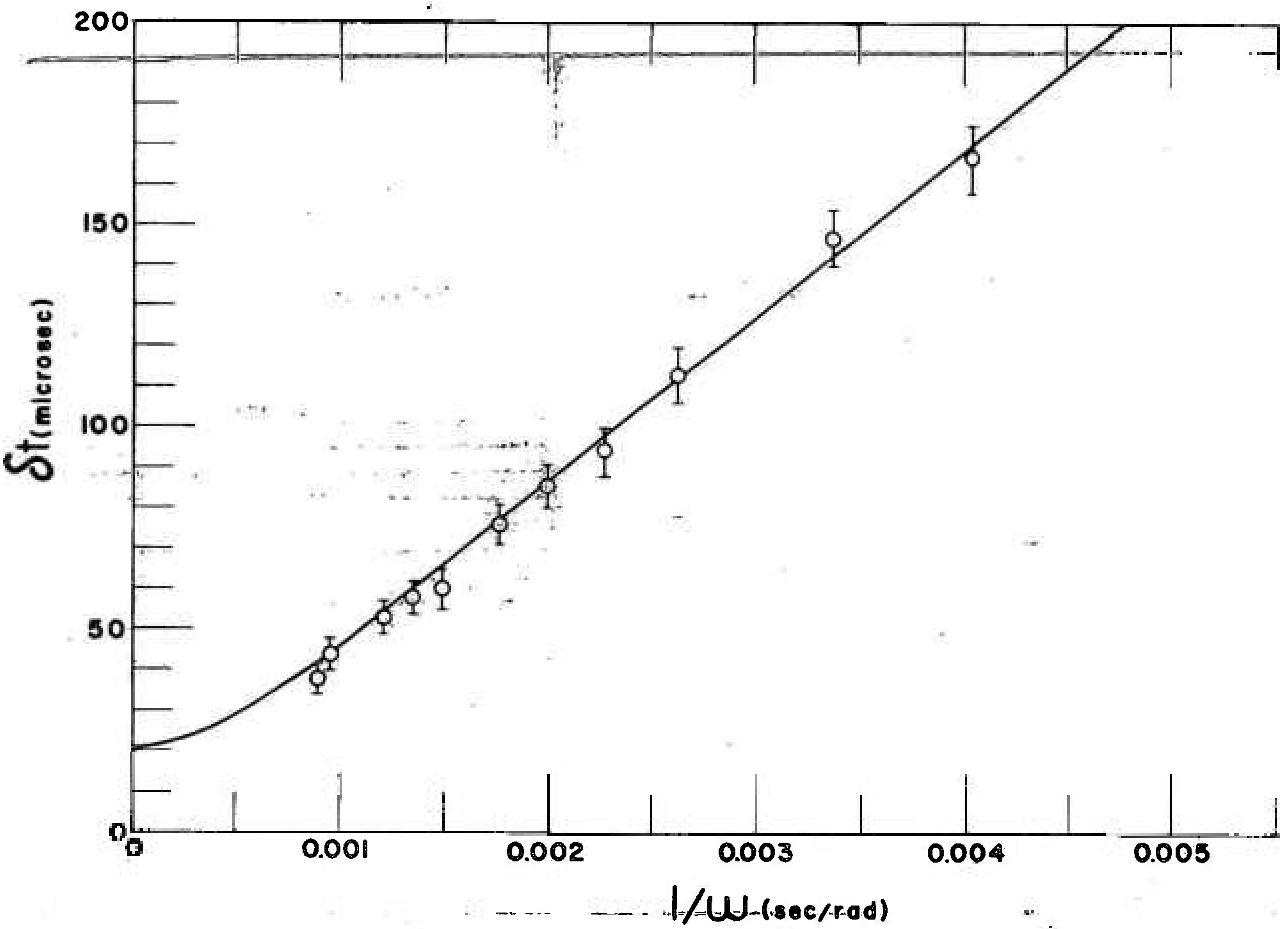

Figure 16 - Spectrometer resolution as a function of $1/\omega$: calculated curve and experimental points.

geometrical thickness d_1 = 1.84cm. The channel width selected in the time analyser was δt_c = 8 μsec. The neutron velocity corresponding to the 110 Bragg cut-off iron is v = 97767cm/sec. Using these values for δt_c and v, the theoretical resolution for a given ω can be calculated by the expression

$$\delta t = \sqrt{\left(\frac{1739}{\omega^2}\right) 10^6 + 418.2} \quad \mu\text{sec} .$$

The experimentally determined resolution width as well as the calculated one versus $1/\omega$ are presented in figure 16. As it can be seen, the agreement between the experimental points and the calculated curve is fairly good.

8. SLOW-NEUTRON TOTAL CROSS SECTION OF GOLD

The total cross-section of gold has been measured for neutrons with wavelengths in the range of 0.95 Å - 7.00 Å, using the apparatus and experimental arrangement already described.

Two different samples have been used: sample 1 with 0.01182 atoms/barn, for measurements in the range 0.95 Å - 2.00 Å, and sample 2 with 0.003903 atoms/barn, for measurements above 2.00 Å. The neutron transmission varied from 0.25 to 0.49 for sample nr. 1, and from 0.23 to 0.63 for sample nr. 2.

An impurity of 0.63% of silver has been determined in sample nr. 2 by activation analysis. The data obtained with this sample have been corrected for this impurity using the following expression for the total cross section of silver (10)

$$\sigma_{Ag} = 6.4 + 9.8/\sqrt{E} = 6.4 + 34.26\lambda$$

with λ , the neutron wavelength, given in Angstroms.

A Fortran Program for data processing, that includes the

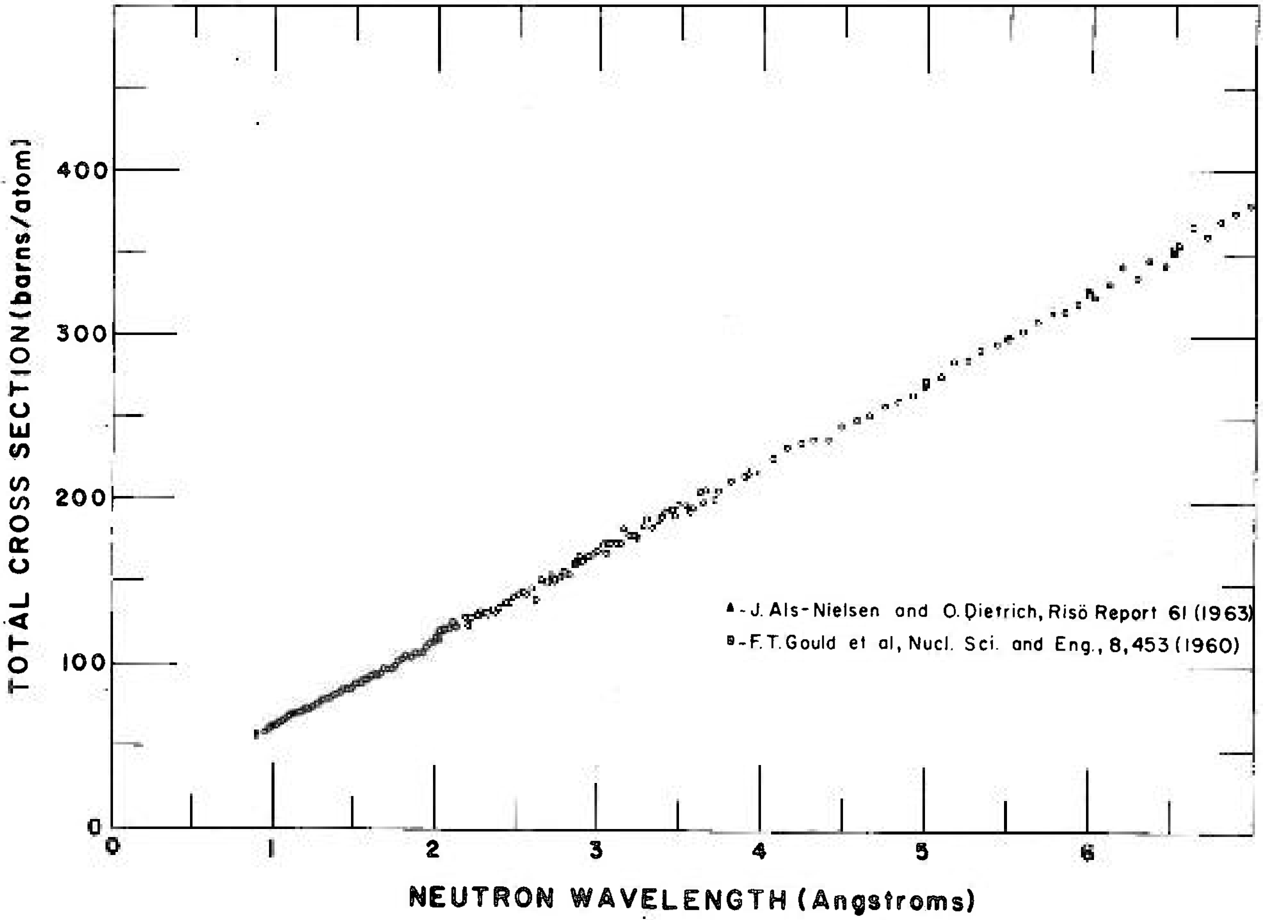

Figure 17 - Total cross section of gold. The statistical errors are smaller or equal to the circles.

total cross-section computation, is given in APPENDIX II.

The wavelength range 0.95 - 7.00 Å has been covered in four different runs as presented in Table II.

TABLE II

Neutron wavelength range (Å)	Sample	Flight Path (meters)	Chopper RPM	Channel length (μsec)
0.95 - 2.00	1	3.00	13970	16
2.03 - 5.78	2	1.49	4090	32
2.25 - 3.70	2	1.49	13170	16
4.00 - 7.00	2	1.49	5740	32

The measured total cross-section of gold as a function of neutron wavelength is presented in figure 17 and in APPENDIX V. The errors indicated are just the statistical ones. These errors are smaller than the circles indicating the experimental results in figure 17, where some previously published data[11][12] are also presented for comparison.

. . .

APPENDIX I

CORRECTIONS FOR COUNTING LOSSES (DEAD TIME)

The formulae that give the correction for counting losses in a detecting system associated to a multichannel time-of-flight analyser, similar to the one utilized in the slow-chopper experiment, have been worked out with detail for channel widths up to 16 microseconds(*).

Three types of counting losses must be considered:

1. Counting losses due to the dead time T of the multichannel time-of-flight analyser (T = 16 μsec, for the TMC analyser utilized).

Let us suppose that, for a certain channel length ΔT and after N_B trigger pulses, the analyser has accumulated a set of counts C_i, i being the channel number. The number of trigger pulses seen by a certain channel will be N_B minus the total number of counts accumulated in the T preceding microseconds. For $\Delta T \leq T$, this correction is carried out by a simple normalization for the real number of trigger pulses, and one gets

$$N_i = C_i \frac{N_B}{N_B - \sum\limits_{j = i - 1}^{j = 1 - T/\Delta T} C_j}$$

where N_i is the corrected, and C_i is the observed number of counts in channel i.

(*) The authors are indebted to S.Paiano Sobrinho and M. C. Paiano, from this Institute, for many clarifying discussions on this problem. They will publish a detailed report on their calculations.

2. Counting losses due to the fact that the analyser registers at most one count per channel per trigger pulse. The possibility of incidence of more than one pulse in a given channel, per analysing cycle, must be taken in account in the correction.

To carry out this correction one needs first to determine the probability, per cycle of analysis, of multiple incidences in one channel. If a Poisson distribution is supposed to apply in the time interval ΔT and if $(a\,\Delta T)$ is the unknown counting rate per channel that reaches the multichannel analyser, it follows that

$$P_1 = \frac{a\,\Delta T}{1\,!}\, e^{-a\,\Delta T}$$ is the probability of one incidence per channel,

$$P_2 = \frac{(a\,\Delta T)^2}{2\,!}\, e^{-a\,\Delta T}$$ is the probability of two incidences per channel,

$$P_3 = \frac{(a\,\Delta T)^3}{3\,!}\, e^{-a\,\Delta T}$$ is the probability of three incidences per channel.

The experimental probability of one, two, and three incidences will be, respectively,

$$P_1 = \frac{N_i}{N_B}\,, \qquad P_2 = \frac{N_{2i}}{N_B}\,, \qquad P_3 = \frac{N_{3i}}{N_B}\,,$$

where N_i, N_{2i}, N_{3i} are, respectively, the number of single, double, and triple incidences, and N_B is the number of possible incidences. Therefore, we have

$$a\,\Delta T\, e^{-a\,\Delta T} = \frac{N_i}{N_B}\,,$$

$$\frac{(a\,\Delta T)^2}{2\,!}\, e^{-a\,\Delta T} = \frac{N_{2i}}{N_B} \quad ,$$

$$\frac{(a\,\Delta T)^3}{3\,!}\, e^{-a\,\Delta T} = \frac{N_{3i}}{N_B} \quad ;$$

and solving for N_{2i} and N_{3i} it follows:

$$N_{2i} = \frac{N_i(a\,\Delta T)}{2\,!} \qquad \text{and} \qquad N_{3i} = N_i \frac{(a\,\Delta T)^2}{3\,!} \; ;$$

The number of real incidences per channel will be $N_i + N_{2i} + N_{3i} + \cdots\cdots$ and therefore

$$N_{ti} = N_i \left(1 + \frac{a\,\Delta T}{2\,!} + \frac{(a\,\Delta T)^2}{3\,!} + \cdots\cdots \right) \quad ,$$

where $a\,\Delta T$ is approximately given by

$$a\,\Delta T \simeq \frac{N_i}{N_B - N_i} \, .$$

3. Counting losses due to the dead time τ of the detector-amplifier-discriminator system preceding the multichannel analyser. First of all this dead time τ will alter the correction formulae for multiple counts, that become

$$N_{ti} = N_i \left(1 + \frac{a}{2!} \frac{(\Delta T - \tau)^2}{\Delta T} + \frac{a^2}{3!} \frac{(\Delta T - 2\tau)^3}{\Delta T} + \cdots\right).$$

After obtaining, by this way, the correct counting rate that reaches the multichannel analyser, one makes the usual correction for the dead time τ :

$$N_{C_i} = \frac{N_{ti}}{1 - R\tau} ,$$

where R is the observed counting rate given by

$$R = \frac{N_{ti}}{N_B \Delta T} .$$

A method has been devised for the counting losses correction when ΔT = 32 μsec = 2T, assuming a linear (non step) distribution of counting rates in two successive channels. Then, in the two halves of channels i and i - 1 we will have the following distribution:

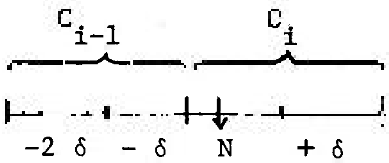

and the following relations will apply:

$$C_{i-1} = 2N - 3\delta \qquad \left\{ \begin{array}{l} \delta = \dfrac{C_i - C_{i-1}}{4} \\ N = \dfrac{3C_i + C_{i-1}}{8} \end{array} \right. \qquad \left\{ N = \dfrac{C_i - \delta}{2} \right.$$

$$C_i = 2N + \delta$$

By making a normalization for each half-channel, we correct for the counting losses due to the dead time T of the multichannel analyser and we get

$$N_i = \frac{N\, N_B}{N_B - (N - \delta)} + \frac{(N + \delta)\, N_B}{N_B - N} , \qquad \text{or}$$

$$N_i = \frac{N_B \times C_i - A}{N_B - \left(\frac{C_i + C_{i-1}}{2}\right) + B},$$

where

$$A = \frac{1}{2}(C_i^2 - \delta^2) - C_i\delta \quad , \qquad B = \frac{C_i^2 - 4\delta C_i + 3\delta^2}{4 N_B}.$$

If the second order terms in δ are neglected we get the simplified expression

$$A = \frac{C_i}{2}\left(\frac{C_i + C_{i-1}}{2}\right) \quad , \qquad B = \frac{C_i\, C_{i-1}}{4\, N_B}$$

or finally

$$N_i = \frac{C_i \left(N_B - \frac{C_i + C_{i-1}}{4} \right)}{N_B - \frac{C_i + C_{i-1}}{2} + \frac{C_i\, C_{i-1}}{4\, N_B}}.$$

For the multiple counting correction in the case in which $T = 32\ \mu$sec, it was assumed that the counting rate in each half-channel corresponds to half the total counting rate for the full channel. In this case the correction must be made on each half-channel. Hence, the same formulae are obtained with the difference that, in this case ΔT is replaced by T and

$$aT = \frac{N_i}{2N_B - N_i}$$

The correction for the dead time τ of the detector--amplifier-discriminator system will be the same as before.

APPENDIX III

FORTRAN PROGRAMS FOR DATA PROCESSING (FORTRAN II-D)

A. Time of flight data processing and total cross-section computation

The following calculations can be carried out for each analyser channel, by the utilization of this program:

- correction for counting losses due to the overall dead time of the electronic system, according to the formulae derived in APPENDIX I.
- normalization of the counting data with respect to counting time or monitor reading.
- subtraction of the measured background.
- total neutron cross-section computation, from transmission measurements.
- calculation of the wavelength for each channel number, according to the overall calibration.

The program is able to process a maximum of 256 channels each run, having lengths from 0.25 to 32 μsec.

Input data is fed into an IBM 1620-II-D computer by means of punched cards. Cards are punched either manually or by using the punched paper tape coming from the multichannel analyser output system, through a tape to card printing punch machine.

The output data can be obtained through a typewriter and, optionally, also in the form of punched cards.

Four computer switches command the program as follows:

all switches off :- data are corrected for counting losses and normalized.

switch 1 on :- background is subtracted.

switch 1 on and
switch 2 off :- measured background is subtracted channel by channel.

switch 1 and 2 on :- the computer calculates an average background using 11 channels, 5 on each side of the nominal channel, this averaged background being subtracted in each channel. To be used when the measured background is relatively flat and presents a high statistical fluctuation.

switch 3 on :- the total cross-section is calculated after correction, normalization and subtraction of background from the counts corresponding to the open beam and the beam transmitted through the sample under study. The wavelength corresponding to each channel number is also calculated.

switch 4 on :- the corrected and normalized counts, and its statistical error, with or without background subtraction depending on the position of switch 1, are obtained in the computer output in the form of punched cards, that can eventually be utilized in other programs. When switch 3 is on, instead of counts the cards deliver the wavelength and cross-section for each channel, with correspondent errors.

There is a variable in the program - the sample indicator - that must assume one of the following values:

M = 1, open beam counts;

M = 2, open beam background counts;

M = 3, counts corresponding to the beam transmitted through the sample;

M = 4, counts corresponding to the background of the beam transmitted through the sample.

In order to process a set of data, the computer must be fed in the following sequence:

1. card containing the general constants of the problem: multichannel analyser dead time, dead time of the detector - amplifier-discriminator system , channel length, number of the first and last channel to be processed and position of the analyser delay switch.

2. card containing the constants of a particular set of counts: total number of bursts (trigger pulses) , normalization factor , chopper speed and sample indicator.

3. cards containing the data to be processed.

4. only for total cross-section computation a card containing: number of atoms of interest per barn in the sample, chopper speed, correction constants due to the presence of other atoms in the sample (with cross-sections of the form $A + B\lambda$), flight path used and the constant for calibration correction.

For background subtraction only items 2 and 3 are repeated for M = 1 and M = 2.

In the case of total cross-section calculation, items 2 and 3 are repeated for M = 1, 2, 3, 4 before item 4.

When a processing cycle is completed the computer returns to the initial position and it is ready to receive and process a new complete set of data.

Besides printing all the constants of the problem for further reference the computer indicates, in the output data, the channel interval in which the dead time correction was greater than 30%. For example, the printing

M = 1 I1 = 37 I2 = 62

indicates that in the open beam counting, between the channels 37 and 62, the dead time correction was greater than 30%.

This program includes the calculation of the statistical errors for the corrected counting as well as for the total cross section. In the first case, column N in the typewriter output data sheet indicates the channel number, column COUNT, the counting and column ERROR, its statistical error. In the second case, column N indicates the channel number, column WL, the wavelength in Å, column CROSS SECTION, the total cross-section in barns and column ERROR, its statistical error, also in barns.

The program in FORTRAN II-D language is presented in the following pages.

B. Chopper - conversion of channel number to neutron time-of--flight, wavelength, and energy.

This program carries out the conversion of channel number to neutron time-of-flight, wavelength, and energy, taking into account the multichannel analyser characteristics described in section 2, and the constant calibration correction Δt_3 mentioned in section 4.

The time-of-flight corresponding to the channel number C, having a width ΔT μsec, is given by

$$t\,(\mu sec) = (C - 0.5)\,\Delta T - (\Delta T - 1) + \Delta t_3 \,,$$

$$\text{for} \quad \Delta T \leq 16\,\mu sec\,;$$

$$t\ (\mu sec) = (C - 0.5)\ \Delta T - 15 + \Delta t_3 \ ,$$

$$\text{for} \quad \Delta T = 32\ \mu sec.$$

The conversion formulae from time to μsec/m, to wavelength (Å) and to energy (ev) are:

$$t^*(\mu sec/m) = t\ (\mu sec)/\ L(m)\ ,$$

where L is the flight path, in meters,

$$\lambda(\text{Å}) = t^*\ (\mu sec/m)\ /\ 252.8302 \quad \text{and}$$

$$E(ev) = 0.081783\ /\ \lambda^2\ (\text{Å})^2\ .$$

An arbitrary number of data can be processed using just one master card containing the channel width in μsec, the flight path in meters, the number of the first and last channel,and the constant calibration correction in μsec.

The typewriter output data sheet gives a table with columns corresponding to channel number, time-of-flight (μsec) , μsec/m, wavelength (Å), and energy (ev).

The following page presents the program in FORTRAN II-D.

```
C      TIME OF FLIGHT DATA PROCESSING AND CROSS SECTION
COMPUTATION
C      TIMES MUST BE GIVEN IN SECONDS
C      MAXIMUM CHANNEL NUMBER IS 256
C      MAXIMUM CHANNEL LENGTH 32 MICROSECONDS
C      T = MULTICHANNEL STORAGE TIME
C      TAU = DEAD TIME OF THE ELECTRONIC DETECTING SYSTEM
C      DELTA= CHANNEL LENGTH
C      N1 = FIRST CHANNEL NUMBER
C      N2 = LAST CHANNEL NUMBER
C      DELAY = DELAY POSITION OF THE MULTICHANNEL
C      BURST = TOTAL NUMBER OF BURSTS
C      FATOR = NORMALIZATION FACTOR
C      RPM = CHOPPER SPEED IN RPM
C      M = SAMPLE INDICATOR
C      Y(I) = TOTAL COUNTING IN EACH CHANNEL
C      CTE = NUMBER OF ATOMS OF INTEREST PER BARN IN THE
SAMPLE
C      CORA AND CORB = COEFFICIENTS FOR THE CORRECTION
DUE TO IMPURITY
C      ATOMS IN THE SAMPLE
C      DIST= FLIGHT PATH IN METERS
C      CAL = ADDITIVE CONSTANT FOR CALIBRATION
       DIMENSION Y(256),F(256),R(256),D(256),ED(256),A(25
6),EA(256)
     1 READ 2,T,TAU,DELTA,N1,N2,DELAY
     2 FORMAT (3E14.8,2I4,I2)
       PRINT 23,DELTA,DELAY
    23 FORMAT (10X,6HDELTA=E14.8,10X,6HDELAY=I2//)
    30 READ 3,BURST,FATOR,RPM,M
     3 FORMAT (F9.0,E14.8,F6.0,I2)
       READ 4, (Y(I),I=N1,N2)
     4 FORMAT (7(4X,F7.0))
       DO 5 I=N1,N2
     5 F(I)=BURST
       IF(T-DELTA)6,7,7
     7 ENE=N1
       M1=T/DELTA+ENE
       DO 8 I=M1,N2
       M2=I-M1+N1
       M3=I-1
       DO 9 J=M2,M3
     9 F(I)=F(I)-Y(J)
     8 CONTINUE
       DO 10 I=M1,N2
       F(I)=BURST/F(I)
       R(I)=Y(I)*F(I)/((BURST-Y(I)*F(I))*DELTA)
       F(I)=F(I)*(1.+(R(I)/2.)*((DELTA-TAU)**2)/DELTA+(R(
I)**2/6.)*((DELT
```

```
     1A-2.*TAU)**3)/DELTA)
      R(I)=(Y(I)*F(I))/(BURST*DELTA)
      F(I)=F(I)/(1.-(R(I)*TAU))
      R(I)=(Y(I)**.5)*(F(I)/FATOR)
   10 Y(I)=Y(I)*(F(I)/FATOR)
      GO TO 11
    6 M1=N1+1
      DO 12 I=M1,N2
      F(I)=F(I)-(Y(I)+Y(I-1))/2.+(Y(I)*Y(I-1))/(4.*BUR
ST)
      F(I)=(BURST-(Y(I)+Y(I-1))/4.)/F(I)
      R(I)=(Y(I)*F(I))/((2.*BURST-Y(I)*F(I))*T)
      F(I)=F(I)*(1.+(R(I)/2.)*((T-TAU)**2)/T+(R(I)**2/
6.)*((T-2.*TAU)**3
     2)/T)
      R(I)=(Y(I)*F(I))/(BURST*DELTA)
      F(I)=F(I)/(1.-(R(I)*TAU))
      R(I)=(Y(I)**.5)*(F(I)/FATOR)
   12 Y(I)=Y(I)*(F(I)/FATOR)
   11 DO 51 I=M1,N2
      IF(F(I)-1.3)51,51,52
   51 CONTINUE
      GO TO 56
   52 I1=I
      DO 53 I=I1,N2
      K=N2+I1-I
      IF(F(K)-1.3)53,53,54
   53 CONTINUE
   54 I2=K
      PRINT 55,M,I1,I2
   55 FORMAT (5X,2HM=I2,5X,3HI1=I4,5X,3HI2=I4/)
   56 IF(SENSE SWITCH 1)13,14
   13 GO TO (14,16,32,33),M
   14 DO 17 I=M1,N2
      D(I)=Y(I)
   17 ED(I)=R(I)
      IF(SENSE SWITCH 1)15,24
   15 IF(SENSE SWITCH 3)30,26
   16 IF(SENSE SWITCH 2)18,19
   18 K1=M1+5
      K2=N2-5
      DO 20 I=K1,K2
      DO 21 J=1,5
      K3=I-J
      K4=I+J
   21 Y(I)=Y(K3)+Y(K4)+Y(I)
      Y(I)=Y(I)/11.
   20 R(I)=(Y(I)/11.)**.5
      IF(M-4)19,35,19
```

```
   19 DO 22 I=M1,N2
      D(I)=D(I)-Y(I)
   22 ED(I)=(ED(I)**2+R(I)**2)**.5
      IF(SENSE SWITCH 3)30,24
   24 IF(SENSE SWITCH 4)25,26
   25 PUNCH 31,(I,D(I),ED(I),I=M1,N2)
   26 PRINT 28,RPM,M,BURST,FATOR
   28 FORMAT (10X,4HRPM=F7.0/10X,2HL=I2/10X,6HBURST=F9.
0/10X,6HFATOR=E14
     3.8//)
      IF(SENSE SWITCH 1)42,41
   42 IF(M-1)41,30,41
   41 PRINT 29
   29 FORMAT (7X,1HN,6X,5HCOUNT,6X,5HERROR,21X,1HN,6X,5
HCOUNT,6X,5HERROR
     9)
      PRINT 31,(I,D(I),ED(I),I=M1,N2)
   31 FORMAT (5X,I4,3X,F8.0,3X,F8.0)
      PAUSE
      GO TO 1
   32 DO 34 I=M1,N2
      A(I)=Y(I)
   34 EA(I)=R(I)
      GO TO 30
   33 IF(SENSE SWITCH 2)18,35
   35 READ 36,CTE,RPM,CORA,CORB,DIST,CAL
   36 FORMAT (E14.8,F6.0,2E14.8,F6.3,F6.2)
      PRINT 38,CTE,CORA,CORB,RPM,DIST,CAL
   38 FORMAT (9X,4HCTE=E14.8,6X,5HCORA=E14.8,6X,5HCORB=
E14.8/9X,4HRPM=F7
     8.0,13X,5HDIST=F6.3,14X,4HCAL=F6.2/)
      PRINT 39
   39 FORMAT (2(5X,1HN,5X,2HWL,3X,13HCROSS SECTION,3X,5
HERROR,3X))
      DELTA=DELTA*1.E6
      EWL=(0.5*DELTA)/(DIST*252.8302)
      DO 37 I=M1,N2
      A(I)=A(I)-Y(I)
      EA(I)=EA(I)**2+R(I)**2
      C=I
      IF(DELTA-16.0)62,62,61
   62 WL=((C-0.5+DELAY*256.)*DELTA-(DELTA-1.0)+CAL)/(DI
ST*252.8302)
      GO TO 43
   61 WL=((C-0.5+DELAY*256.)*DELTA-15.0+CAL)/(DIST*252.
8302)
   43 Y(I)=(LOGF(D(I)/A(I)))/CTE-(CORA+CORB*WL)
      R(I)=((ED(I)/D(I))**2+EA(I)/(A(I)**2))**.5/CTE
```

```
      IF(SENSE SWITCH 4)70,37
   70 PUNCH 71,WL,EWL,Y(I),R(I)
   71 FORMAT (4(E14.8))
   37 PRINT 40,I,WL,Y(I),R(I)
   40 FORMAT (3X,I4,1X,F7.3,1X,E12.6,1X,E11.5)
      PAUSE
      GO TO 1
      END

30602 CORES USED
39999 NEXT COMMON
END OF COMPILATION
EXECUTION
```

```
C     CHOPPER-CONVERSION OF CHANNEL NUMBER IN TIME OF
FLIGHT,
C     NEUTRON WAVELENGTH AND ENERGY.
C     DELTA=CHANNEL LENGTH IN MICROSECONDS
C     DIST = FLIGHT PATH IN METERS
C     CAL=CONSTANT CALIBRATION CORRECTION
C     N1=FIRST CHANNEL
C     N2=LAST CHANNEL
C     C=I=NUMBER OF CHANNEL
C     TMS=TIME OF FLIGTH IN MICROSECONDS
C     TMSM=TIME OF FLIGTH IN MICROSECONDS/METER
C     WL=NEUTRON WAVELENGTH IN ANGSTRONS
C     E=ENERGY IN EV
    1 READ 100,DELTA,DIST,N1,N2,CAL
      PRINT 101,DELTA,DIST,CAL
      PRINT 102
      IF(DELTA-16.0)2,2,3
    2 DO 10 I=N1,N2
      C=I
      TMS=(C-0.5)*DELTA-(DELTA-1.0)+CAL
      TMSM=TMS/DIST
      WL=TMSM/252.8302
      E=0.081783/(WL*WL)
      PRINT 103,I,TMS,TMSM,WL,E
   10 CONTINUE
      GO TO 4
    3 DO 20 I=N1,N2
      C=I
      TMS=(C-0.5)*DELTA-15.0+CAL
      TMSM=TMS/DIST
      WL=TMSM/252.8302
      E=0.081783/(WL*WL)
      PRINT 103,I,TMS,TMSM,WL,E
   20 CONTINUE
    4 PAUSE
      GO TO 1
  100 FORMAT (F4.0,F7.4,2I4,F6.2)
  101 FORMAT (25X,23HTABLE OF CONVERSION FOR/30X,6HDELT
A=F4.0/30X,5HDIST
     1=F7.4/30X,4HCAL=F6.2/)
  102 FORMAT (8X,1HI,11X,3HTMS,12X,4HTMSM,12X,2HWL,13X,
6HENERGY//)
  103 FORMAT (6X,I4,6X,F9.3,6X,F9.3,8X,F8.3,8X,E11.5)
      END
01728 CORES USED
39999 NEXT COMMON
END OF COMPILATION
EXECUTION
```

APPENDIX III

EFFECT OF THE SPECTROMETER RESOLUTION ON A BRAGG CUT-OFF

The resolution of the spectrometer affects the observed Bragg break in a total cross-section curve of a polycrystalline substance in such a way that the otherwise sharp edges become rounded and the vertical discontinuity assumes a finite slope.

The middle-point of the observed break could be considered as corresponding to the cut-off wavelength given by the Bragg equation, if the total cross-section curve were symmetric about this wavelength. Nevertheless, this is not always the case, mainly for the last break, after which coherent scattering no longer exists. Therefore, if a Bragg break is going to be used as a calibration reference for the time-of-flight or wavelength scale, care should be taken to determine accurately the point on the total cross-section curve that corresponds, for a given resolution, to twice the calculated interplanar spacing of the planes hkl under consideration[3].

If the incident spectrum $D(\lambda)$ and the theoretical total cross-section $\sigma_t(\lambda)$ are known, the neutron spectrum trasmitted through the sample can be determined by the expression

$$A(\lambda) = D(\lambda)\, e^{-n\,\sigma_t(\lambda)} \quad ,$$

where n is the number of atoms per barn in the sample.

The incident spectrum has been measured and it was found that the equation that gives the best fit is(*)

$$D(\lambda) = \frac{30420}{\lambda^{4.039}} \; e^{-\left(\frac{1.640}{\lambda}\right)^2}$$

(*) to be published

Our calibration studies have been performed using the Fe(110) Bragg cut-off, and the total cross-section as a function of neutron wavelength has been calculated(*) in the range of interest by adding the absorption and the scattering cross - -sections (nuclear and magnetic, elastic and inelastic, coherent and incoherent).

When we perform a cross-section measurement, the observed $\bar{\sigma}_t$ will be depend on the spectrometer resolution $R(\lambda)$ according to

$$\bar{\sigma}_t(\lambda_o) = \frac{1}{n} \frac{\int D(\lambda)\, R_{\lambda_o}(\lambda)\, d\lambda}{\int A(\lambda)\, R_{\lambda_o}(\lambda)\, d\lambda} ,$$

where $R_{\lambda_o}(\lambda)$ is the resolution function centered at any particular value λ_o.

In this way the total cross-section curve affected by the resolution was calculated by numerical approximation . The resolution function has been considered of a Gaussian shape, but falling down to zero when the abcissa is twice its half width . Actually the resolution width varies with λ , but this has not been taken into account, since in the interval of interest , between 3 and 5 Å, this variation is less than 5%.

The spectra and the resolution can be converted to time scale, and have been considered distributed in channels, the intervals in time being the actual channel width used for the measurements in the multichannel analyser.

Many curves of total cross-section have been calculated for different resolution widths, using a value 0.10 atoms / barn. The samples measured had n values of this order. Some of the resulting curves are shown in figure 18.

(*) to be published

Analysing these calculated curves, it is observed that the calibration point corresponding to the Fe(110) Bragg cut-off varies with the resolution as shown in Table III, where the ratio between the cross-section at calibration point and the lowest cross-section as well as the position of the calibration point in percents of the total height of the Bragg break are presented. According to Egelstaff[(3)] in an extreme case of a large break or very thick sample a reciprocal transmission of about twice the minimum value would be measured at the calibration point.

We conclude that when performing a spectrometer calibration we must determine for each rotation speed (or resolution) the exact position on the cross-section curve that corresponds to the calibration point.

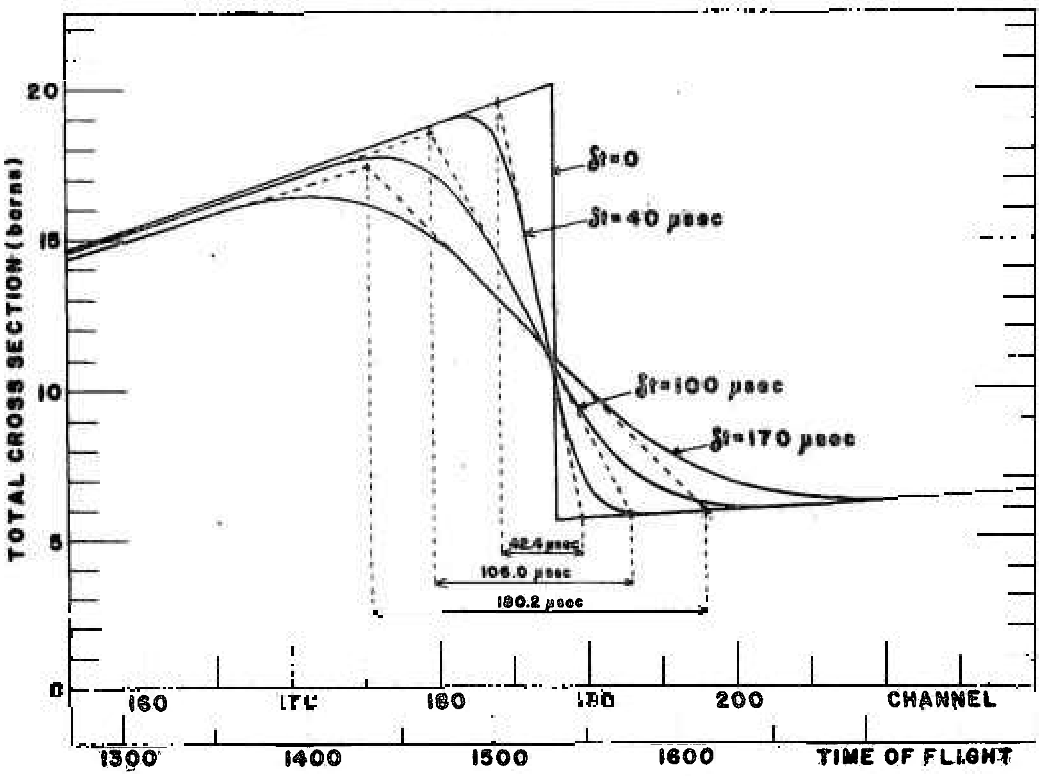

Figure 18 - Effect of the resolution on a Bragg cut-off.

TABLE III

Resolution (microsec.)	Cross-Section at Calibration Point Divided by Lowest Cross-Section	Position of the Calibration Point in Percents of Total Height of the Bragg Break
40	1.78	32.1%
50	1.80	33.2%
60	1.81	34.4%
70	1.83	35.6%
80	1.84	36.7%
90	1.84	37.7%
100	1.85	38.5%
110	1.85	39.4%
120	1.85	40.2%
130	1.85	41.1%
140	1.85	41.9%
150	1.85	42.7%
160	1.85	43.6%
170	1.85	44.4%
180	1.85	45.3%
190	1.85	46.2%

We could observe also that the projection on the time axis of the tangent at the point of inflexion of the sloping cut--off is equal to 1.06 times the half width of the applied resolution, as it has been pointed out by Larsson et al[4]. This is an accurate method for determining experimentally the spectrometer resolution.

These numerical calculations have been performed by an IBM-1620-II-D computer and the program in FORTRAN-II-D language also presented.

```
C     EFFECT OF RESOLUTION ON ONE THEORETICAL CURVE OF
CROSS SECTION
C     RESOLUTION IS ASSUMED IN THE GAUSSIAN FORM
C     DT=RESOLUTION IN TIME(MICROSECONDS)=WIDTH AT HALF
 MAXIMUM
C     DELTA=WIDTH OF CHANNEL
C     N1=FIRST CHANNEL
C     N2=LAST CHANNEL
C     D(I)=COUNTS IN THE CHANNEL I OF ESPECTRUM
C     SIGMA(I) = THEORETICAL CROSS SECTION FOR THE CHAN
NEL I
C     ENE=CONSTANT FOR CROSS SECTION CALCULATION
      DIMENSION F(200),D(280),DI(280),DR(280),SIGMA(280
),A(280),AI(280),
     1AR(280)
    1 READ 100,DT,DELTA
      RES=DT/DELTA
      K1=RES+1.0
      K=4*K1+1
      CM=K1
      SUBT=2.0*CM+1.0
      SUM=0.
      DO 10 I1=1,K
      X=I1
      C=X-SUBT
      F(I1)=1.0/EXPF((C*C)/(0.36075*RES*RES))
      SUM=SUM+F(I1)
   10 CONTINUE
      READ 101,N1,N2
      READ 102, (D(I),I=N1,N2)
      M1=N1+2*K1
      M2=N2-2*K1
      DO 20 I=M1,M2
      L1=I-2*K1
      L2=I+2*K1
      DO 30 J=L1,L2
      L=J+1-L1
   30 DI(L)=D(J)
      DR(I)=0.
      DO 20 M=1,K
      PR=(F(M)*DI(M))/SUM
   20 DR(I)=DR(I)+PR
      READ 103,ENE
      READ 104, (SIGMA(I),I=N1,N2)
      DO 40 I=N1,N2
   40 A(I)=D(I)/EXPF(ENE*SIGMA(I))
      DO 50 I=M1,M2
```

```
      L1=I-2*K1
      L2=I+2*K1
      DO 60 J=L1,L2
      L=J+1-L1
   60 AI(L)=A(J)
      AR(I)=0.
      DO 50 M=1,K
      PR=(F(M)*AI(M))/SUM
   50 AR(I)=AR(I)+PR
      PRINT 105
      DO 70 I=M1,M2
      SIGMAR=LOGF(DR(I)/AR(I))/ENE
   70 PRINT 106,I,SIGMAR
      PAUSE
      GO TO 1
  100 FORMAT (F7.2,F4.0)
  101 FORMAT (2I4)
  102 FORMAT (7(3X,F7.0))
  103 FORMAT (E14.8)
  104 FORMAT (7(1X,F9.3))
  105 FORMAT (24X,36HCROSS SECTION AFFECTED BY RESOLUTI
ON//4(7X,1HI,3X,9
     2HSIGMA RES))
  106 FORMAT (5X,I4,2X,F9.3)
      END

25478 CORES USED
39999 NEXT COMMON
END OF COMPILATION
EXECUTION
```

APPENDIX IV

CALCULATION OF THE FUNCTION $I(\alpha', v_o)$ FOR $\frac{2D}{L} \leq \frac{d}{r}$

The intensity transmitted through the chopper is given, for the neutron velocity, v_o, by

$$I(\alpha') = \int_{\alpha' - \frac{d}{r}}^{\alpha' + \frac{d}{r}} T(\alpha - \alpha')\, I_o(\alpha)\, d\alpha \quad ,$$

where $T(\alpha - \alpha')$ is a triangular function with a basis 2d/r and symmetrical about α', and $I_o(\alpha)$ is a rectangular function with a basis 2D/L.

The function $I_o(\alpha)$ when normalized is given by

$$I_o(\alpha) \begin{cases} = 1, \text{ for } |\alpha| \leq D/L \\ = 0, \text{ for } |\alpha| \geq D/L \end{cases}$$

If the area of the triangle defined by $T(\alpha - \alpha')$ is normalized to unity, this function becomes

$$T(\alpha - \alpha') = \frac{r}{d}\left(1 - \frac{r}{d}\,|\alpha - \alpha'|\right) .$$

The resultant $I(\alpha')$ has a non zero value in the interval

$$-\left(\frac{D}{L} + \frac{d}{r}\right) \leq \alpha' \leq \left(\frac{D}{L} + \frac{d}{r}\right) .$$

The maximum transmission is obtained for $\alpha' = 0$, and is given by the dashed area of figure 19(a) that is equal to the total area (unity) minus the sum of the excluded partial areas

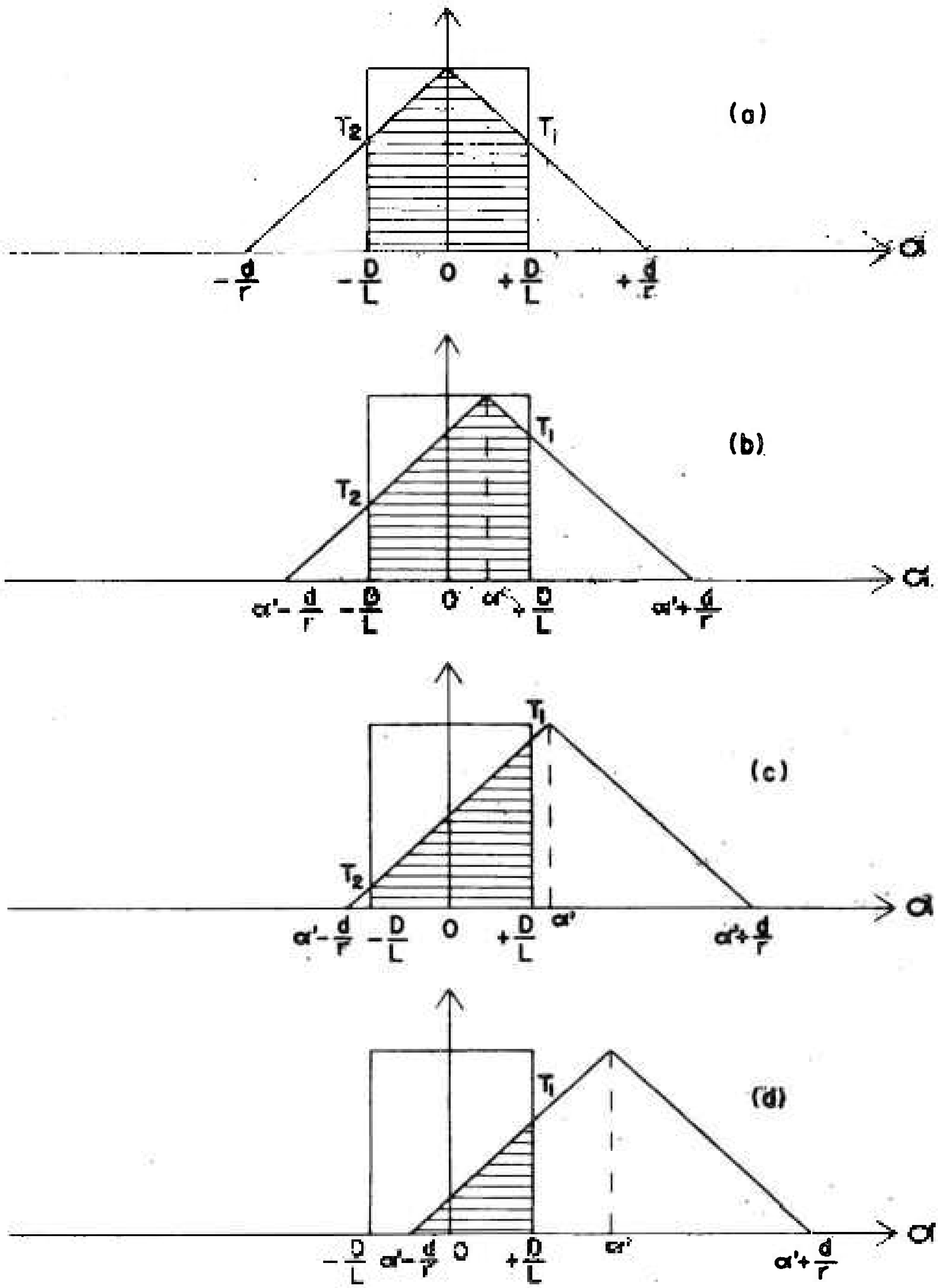

Figure 19 - The dashed areas represent the function $I(\alpha', v_o)$ for $\frac{2D}{L} \leq \frac{d}{r}$.

$$I_{max} = 1 - 2 \{ \frac{1}{2} (\frac{d}{r} - \frac{D}{L}) T (\frac{D}{L} - 0) \}$$

or

$$I_{max} = 1 - (\frac{d}{r} - \frac{D}{L}) \frac{r}{d} (1 - \frac{r}{d} \frac{D}{L})$$

and, hence $I_{max} = 1 - (\frac{r}{d})^2 (\frac{d}{r} - \frac{D}{L})^2$ that is always less than 1 for $\frac{2D}{L} \leq \frac{d}{r}$. The màximum transmission can arrive only to 75% in this case.

Let us study the functional behaviour of the resultant $I(\alpha')$:

1) In the interval $0 \leq |\alpha'| \leq \frac{D}{L}$ (figure 19(b)) it becomes

$$I(\alpha') = 1 - \frac{1}{2} \left[T_1(\alpha')(\frac{d}{r} - \frac{D}{L} + \alpha') + (\frac{d}{r} - \frac{D}{L} - \alpha') T_2(\alpha') \right]$$

where

$$T_1(\alpha') = \frac{r}{d} \left[1 - \frac{r}{d} (\frac{D}{L} - \alpha') \right] \quad , \quad T_2(\alpha') = \frac{r}{d} \left[1 - \frac{r}{d} (\frac{D}{L} + \alpha') \right]$$

and hence

$$I(\alpha') = 1 - (\frac{r}{d})^2 \left[(\frac{d}{r} - \frac{D}{L})^2 + \alpha'^2 \right] \qquad (1)$$

that is reduced to I_{max} for $\alpha' = 0$.

2) In the interval $\frac{D}{L} \leq |\alpha'| \leq \frac{d}{r} - \frac{D}{L}$ (figure 19(c)):

$$I(\alpha') = \frac{1}{2} \left[(\frac{d}{r} - \alpha' + \frac{D}{L}) T_1(\alpha') - (\frac{d}{r} - \alpha' - \frac{D}{L}) T_2(\alpha') \right] ,$$

where

$$T_1(\alpha') = \frac{r}{d} \left[1 - \frac{r}{d} (\alpha' - \frac{D}{L}) \right] \quad ,$$

$$T_2(\alpha') = \frac{r}{d}\left[1 - \frac{r}{d}\left(\alpha' + \frac{D}{L}\right)\right]$$

and, therefore

$$I(\alpha') = \left(\frac{r}{d}\right)^2 \left\{2\frac{D}{L}\left(\frac{d}{r} - \alpha'\right)\right\} \qquad (2)$$

Expressions (1) and (2) coincide for $|\alpha'| = \frac{D}{L}$, with the result

$$I\left(\frac{D}{L}\right) = 2\frac{r}{d}\frac{D}{L}\left(1 - \frac{r}{d}\frac{D}{L}\right).$$

3) In the interval $\frac{d}{r} - \frac{D}{L} \leq |\alpha'| \leq \frac{d}{r} + \frac{D}{L}$ (figure 19(d)):

$$I(\alpha') = \frac{1}{2}\left(\frac{d}{r} - \alpha' + \frac{D}{L}\right) T_1(\alpha') \quad ,$$

where

$$T_1(\alpha') = \frac{r}{d}\left[1 - \frac{r}{d}\left(\alpha' - \frac{D}{L}\right)\right] \quad , \text{ and hence}$$

$$I(\alpha') = \frac{1}{2}\left(\frac{r}{d}\right)^2\left(\frac{d}{r} - \alpha' + \frac{D}{L}\right)^2 . \qquad (3)$$

Expressions (2) and (3) coincide for $|\alpha'| = \frac{d}{r} - \frac{D}{L}$, and we have

$$I\left(\frac{d}{r} - \frac{D}{L}\right) = 2\cdot\frac{r^2}{d^2}\frac{D^2}{L^2} .$$

In order to determine the full width at half maximum $2\bar{\alpha}$ so that $I(\bar{\alpha}) = I_{max}/2$, we must know in which branch of the curve it can be found.

Let us compare the values $I_{max}/2$ and $I(\frac{D}{L})$.

$$\frac{I_{max}}{2} = \frac{r}{d}\frac{D}{L}\left(1 - \frac{1}{2}\frac{r}{d}\frac{D}{L}\right) \quad \therefore \quad \frac{I_{max}}{2} = k\left[1 - \frac{1}{2}\frac{r}{d}\frac{D}{L}\right] \text{ and}$$

$$I(\frac{D}{L}) = \frac{r}{d}\ \frac{D}{L}(2 - 2\frac{r}{d}\ \frac{D}{L}) \quad \therefore \quad I(\frac{D}{L}) = k\left[1 - (2\frac{r}{d}\frac{D}{L} - 1)\right] .$$

Let us now compare the values $A = \frac{1}{2}\frac{r}{d}\frac{D}{L}$ and $B = 2\frac{r}{d}\frac{D}{L} - 1$.

As $\frac{2D}{L} \leq \frac{d}{r}$, we have $\frac{2D}{L}\ \frac{r}{d} \leq 1$ and therefore $B \leq 0$. But $A > 0$ and so $A > B$, and hence $I(\frac{D}{L}) > I_{max}/2$, and $\bar{\alpha}$ must be in the interval $\frac{D}{L} \leq \bar{\alpha} \leq \frac{D}{L} + \frac{d}{r}$.

Let us compare the values $I_{max}/2$ and $I(\frac{d}{r} - \frac{D}{L})$

$$\frac{I_{max}}{2} = \frac{r}{d}\ \frac{D}{L}\ (1 - \frac{1}{2}\frac{r}{d}\frac{D}{L}) \qquad \text{and}$$

$$I(\frac{d}{r} - \frac{D}{L}) = \frac{r}{d}\ \frac{D}{L}\ (2\frac{r}{d}\ \frac{D}{L}) .$$

If we call $C = \frac{r}{d}\ \frac{D}{L}$ and $\begin{cases} A = 1 - \frac{C}{2} \\ B = 2C \end{cases}$ it results

$A \leq B$ for $1 - \frac{C}{2} \leq 2C$ or $C \geq \frac{2}{5}$, and hence $\frac{2D}{L} \geq \frac{4}{5}\frac{d}{r}$

$A \geq B$ for $1 - \frac{C}{2} \geq 2C$ or $C \leq \frac{2}{5}$, and hence $\frac{2D}{L} \leq \frac{4}{5}\frac{d}{r}$.

It is concluded that, for $\frac{4}{5}\frac{d}{r} \leq \frac{2D}{L} \leq \frac{d}{r}$:

$$\frac{d}{r} - \frac{D}{L} \leq \bar{\alpha} \leq \frac{d}{r} + \frac{D}{L}$$

and for $\frac{2D}{L} \leq \frac{4}{5}\ \frac{d}{r}$:

$$\frac{D}{L} \leq \bar{\alpha} \leq \frac{d}{r} - \frac{D}{L} .$$

Let us determine the full width at half maximum for the two cases:

a) $\frac{4}{5}\frac{d}{r} \leq \frac{2D}{L} \leq \frac{d}{r}$

$$I(\bar{\alpha}) = \frac{1}{2}\left(\frac{r}{d}\right)^2\left(\frac{d}{r} - \bar{\alpha} + \frac{D}{L}\right)^2 = \frac{r}{d}\frac{D}{L}\left(1 - \frac{1}{2}\frac{r}{d}\frac{D}{L}\right) .$$

By expansion of the above expression we obtain an equation of the second degree in $\bar{\alpha}$ from which just the negative root is solution of the problem.

The following result is obtained:

$$2\bar{\alpha} = 2\left(\frac{d}{r} + \frac{D}{L}\right) - 2\sqrt{\frac{D}{L}\left(\frac{2d}{r} - \frac{D}{L}\right)}$$

In this case:

$$1.2\frac{d}{r} \leq 2\bar{\alpha} \leq (3 - \sqrt{3})\frac{d}{r} .$$

b) $\frac{2D}{L} \leq \frac{4}{5}\frac{d}{r}$

$$I(\bar{\alpha}) = \left(\frac{r}{d}\right)^2\left[2\frac{D}{L}\left(\frac{d}{r} - \bar{\alpha}\right)\right] = \frac{r}{d}\frac{D}{L}\left(1 - \frac{1}{2}\frac{r}{d}\frac{D}{L}\right) .$$

It follows that $2\bar{\alpha} = \frac{d}{r} + \frac{D}{2L}$ and the full width at half maximum in this case has an upper limit $2\bar{\alpha} \leq 1.2\frac{d}{r}$.

We have derived the resolution function and its full width at half maximum for the case $\frac{2D}{L} \leq \frac{d}{r}$.

It is of interest to calculate the integral of this curve, given by

$$I = 2\,(I_1 + I_2 + I_3) , \qquad \text{where}$$

$$I_1 = \int_0^{D/L} \left\{ 1 - \left(\frac{r}{d}\right)^2 \left[\left(\frac{d}{r} - \frac{D}{L}\right)^2 + \alpha^2 \right] \right\} d\alpha ,$$

$$I_2 = \int_{D/L}^{d/r - D/L} \left(\frac{r}{d}\right)^2 \frac{2D}{L} \left(\frac{d}{r} - \alpha\right) d\alpha \quad \text{and}$$

$$I_3 = \int_{d/r - D/L}^{d/r + D/L} \frac{1}{2} \left(\frac{r}{d}\right)^2 \left(\frac{d}{r} - \frac{D}{L} - \alpha\right)^2 d\alpha .$$

By straightforward calculus we get

$$I_1 = \frac{2r}{d} \left(\frac{D}{L}\right)^2 - \frac{4}{3} \left(\frac{r}{d}\right)^2 \left(\frac{D}{L}\right)^3 ,$$

$$I_2 = \frac{D}{L} - 2 \frac{r}{d} \left(\frac{D}{L}\right)^2 ,$$

$$I_3 = \frac{4}{3} \left(\frac{r}{d}\right)^2 \left(\frac{D}{L}\right)^3 .$$

and hence

$$I = 2 \frac{D}{L}$$

This area is independent of the chopper opening and is equal, as it could be expected, to the area of the function $I_o(\alpha)$ with an unity value.

APPENDIX V

MEASURED TOTAL NEUTRON CROSS SECTION OF GOLD AS A FUNCTION OF NEUTRON WAVELENGTH AND STATISTICAL ERRORS

Neutron Wavelength	Total Cross Section	Neutron Wavelength	Total Cross Section
0.95	59.6 ± 0.4	1.48	85.7 ± 0.4
0.98	61.8 ± 0.4	1.50	86.3 ± 0.4
1.00	61.8 ± 0.4	1.52	88.9 ± 0.4
1.02	63.9 ± 0.4	1.55	89.3 ± 0.4
1.04	65.1 ± 0.3	1.57	90.8 ± 0.4
1.06	65.3 ± 0.3	1.59	90.5 ± 0.4
1.08	66.7 ± 0.3	1.61	92.9 ± 0.4
1.10	68.1 ± 0.3	1.63	94.0 ± 0.4
1.12	69.6 ± 0.3	1.65	93.5 ± 0.4
1.14	70.7 ± 0.3	1.67	95.5 ± 0.4
1.17	70.7 ± 0.3	1.69	97.1 ± 0.4
1.19	71.9 ± 0.3	1.71	98.0 ± 0.5
1.21	72.5 ± 0.3	1.74	97.9 ± 0.5
1.23	73.0 ± 0.3	1.76	99.9 ± 0.5
1.25	75.2 ± 0.3	1.78	101.9 ± 0.5
1.27	75.7 ± 0.3	1.80	103.7 ± 0.5
1.29	76.8 ± 0.3	1.82	104.7 ± 0.5
1.31	78.7 ± 0.3	1.84	106.4 ± 0.5
1.33	79.0 ± 0.3	1.86	105.3 ± 0.5
1.36	80.1 ± 0.3	1.88	107.3 ± 0.5
1.38	81.2 ± 0.4	1.90	106.8 ± 0.6
1.40	82.2 ± 0.4	1.93	107.0 ± 0.6
1.42	82.9 ± 0.4	1.95	111.2 ± 0.6
1.44	85.0 ± 0.4	1.97	112.5 ± 0.6
1.46	84.4 ± 0.4	1.99	114.3 ± 0.6

Neutron Wavelength	Total Cross Section	Neutron Wavelength	Total Cross Section
2.01	117.6 ± 0.7	2.88	166 ± 1
2.03	121 ± 1	2.90	163 ± 2
2.05	121 ± 1	2.94	166 ± 2
2.09	122 ± 1	2.96	167 ± 1
2.11	126 ± 1	2.99	169 ± 2
2.14	123 ± 1	3.03	173 ± 2
2.18	129 ± 1	3.05	168 ± 1
2.20	124 ± 1	3.07	174 ± 2
2.22	129 ± 1	3.11	174 ± 2
2.26	130 ± 1	3.13	174 ± 1
2.28	131 ± 1	3.16	183 ± 2
2.31	131 ± 1	3.20	179 ± 2
2.35	134 ± 1	3.22	179 ± 1
2.37	133 ± 1	3.24	178 ± 2
2.39	135 ± 1	3.28	185 ± 2
2.43	138 ± 1	3.30	189 ± 1
2.45	138 ± 1	3.33	184 ± 2
2.48	141 ± 1	3.37	188 ± 2
2.52	143 ± 1	3.39	190 ± 1
2.54	144 ± 1	3.41	194 ± 2
2.56	143 ± 1	3.45	195 ± 2
2.60	147 ± 1	3.47	191 ± 1
2.62	140 ± 1	3.49	198 ± 2
2.65	152 ± 1	3.54	198 ± 2
2.69	150 ± 1	3.56	193 ± 1
2.71	155 ± 1	3.58	196 ± 2
2.73	152 ± 2	3.62	206 ± 2
2.77	156 ± 2	3.64	200 ± 2
2.79	157 ± 1	3.66	207 ± 3
2.82	156 ± 2	3.71	201 ± 3
2.86	163 ± 2	3.73	207 ± 2

Neutron Wavelength	Total Cross Section	Neutron Wavelength	Total Cross Section
3.81	212 ± 2	5.43	296 ± 2
3.90	216 ± 2	5.51	301 ± 3
3.98	218 ± 2	5.60	304 ± 3
4.07	226 ± 1	5.68	310 ± 2
4.15	233 ± 2	5.77	315 ± 2
4.24	236 ± 2	5.85	316 ± 2
4.32	238 ± 1	5.94	320 ± 2
4.41	238 ± 2	6.02	324 ± 2
4.49	246 ± 1	6.11	332 ± 2
4.58	250 ± 2	6.19	343 ± 2
4.66	253 ± 1	6.28	336 ± 2
4.75	258 ± 1	6.36	346 ± 3
4.83	261 ± 1	6.45	343 ± 3
4.92	265 ± 1	6.53	356 ± 3
5.00	271 ± 1	6.62	366 ± 3
5.09	277 ± 1	6.70	360 ± 3
5.17	285 ± 2	6.79	368 ± 3
5.26	286 ± 2	6.87	375 ± 3
5.34	293 ± 2	6.96	380 ± 3

The neutron wavelength is given in Angstroms and the total cross-section in barns.

ACKNOWLEDGEMENTS

The authors wish to thank Professor M.D. de Souza Santos for valuable discussions and encouragement during the development of the project, Professor K.E. Larsson, from the Royal Institute of Technology, Stockholm, who kindly made available the design of the slow-chopper and stimulated us to pursue this line of experiments and Dr. R.L. Zimmerman, from the Instituto Tecnológico da Aeronáutica, São José dos Campos, for his aid during the course of the experiments.

We are also indebted to Mr. José Ferreira for the construction of the slow-chopper and to the Reactor Operation Division for the routine and special operations of the IEAR-1 Reactor.

REFERENCES

1. D.J. Hughes, Pile Neutron Research (Addison-Wesley, 1953), pp 243-254.
2. E. Fermi, J. Marshall and L. Marshall, Phys. Rev. 72, 193 (1947).
3. P.A. Egelstaff, J. Nucl. Energy 1, 57 (1954).
4. K.E. Larsson, U. Dahlborg, S.Holmryd, K. Otnes and R. Stedman, Arkiv för Fysik Band 16, nr.19, 199 (1959).
5. T. Niewiadomski, A. Szkatula and J. Sciesinski, Nukleonika VII nr.4, 231 (1962).
6. K.E. Larsson, R. Stedman and H. Palevsky, J. Nucl. Energy 6 , 222 (1958).
7. Directory of Nuclear Reactors, vol. III (IAEA 1960), pp 25--26.
8. M. Damy de Souza Santos and P. Saraiva de Toledo, Proc. of the 2nd International Conference on the Peaceful Uses of the

Atomic Energy, P/2274, vol.10 (United Nations 1958), pp 259.

9. M. Marseguerra and G. Pauli, Nucl. Instr. & Method 4 , 140 (1959).

10. T.I. Taylor and W.W. Havens Jr., "Neutron Spectroscopy and Neutron Interaction in Chemical Analysis" in Physical Methods in Chemical Analysis, vol. III (Walter G.Berl, Academic Press 1956).

11. F.T. Gould, T.I. Taylor, W.W. Havens Jr., B.M. Rustad and E. Melkonian, Nucl. Sci. and Eng. 8, 453 (1960).

12. J. Als-Nielsen and O. Dietrich, Risö Report nr.61 (July (1963).

. . .